LAPPEENRANTA UNIVERSITY OF TECHNOLOGY
Faculty of Technology
Degree Programme in Energy Technology

Juha Luukka

IMPROVING THE CALCULATION OF RATE OF STRATIFICATION IN APROS

Examiners: Prof. Riitta Kyrki-Rajamäki
Dr. Tech. Markku Hänninen

Instructor: Dr. Tech. Markku Hänninen

ABSTRACT

Lappeenranta University of Technology

Faculty of Technology

Degree Programme in Energy Technology

Juha Luukka

Improving the calculation of rate of stratification in APROS

Master's thesis
2010

72 pages, 43 figures and 2 appendices

Examiners: Prof. Riitta Kyrki-Rajamäki
Dr. Tech. Markku Hänninen

Instructor: Dr. Tech. Markku Hänninen

Keywords: APROS, interfacial friction, flow regime, channel inclination, flow stratification, six-equation model, two-phase flow.

APROS (Advanced Process Simulation Environment) is a computer simulation program developed to simulate thermal hydraulic processes in nuclear and conventional power plants. Earlier research at VTT Technological Research Centre of Finland had found the current version of APROS to produce inaccurate simulation results for a certain case of loop seal clearing. The objective of this Master's thesis is to find and implement an alternative method for calculating the rate of stratification in APROS, which was found to be the reason for the inaccuracies.

Brief literature study was performed and a promising candidate for the new method was found. The new method was implemented into APROS and tested against experiments and simulations from two test facilities and the current version of APROS. Simulation results with the new version were partially conflicting; in some cases the new method was more accurate than the current version, in some the current method was better. Overall, the new method can be assessed as an improvement.

TIIVISTELMÄ

Lappeenrannan teknillinen yliopisto

Teknillinen tiedekunta

Energiatekniikan osasto

Juha Luukka

Prosessisimulaattori APROS:n kerrostumisasteen laskennan kehittäminen

Diplomityö
2010

72 sivua, 43 kuvaa ja 2 liitettä

Tarkastajat: Prof. Riitta Kyrki-Rajamäki
TkT Markku Hänninen

Ohjaaja: TkT Markku Hänninen

Avainsanat: APROS, faasien välinen kitka, kaksifaasivirtaus, kanavan kaltevuus, kuusiyhtälömalli, virtauksen kerrostuneisuus, virtausmuoto.

APROS (Advanced Process Simulation Environment) on simulaatio-ohjelmisto, joka on kehitetty voimalaitosten termohydraulisten prosessien mallintamiseen. Aiemmassa tutkimuksessa VTT:llä havaittiin ydinvoimalaitoksen vesilukon avautumisen laskennan olevan tietyssä tapauksessa epätarkkaa. Tämän diplomityön tavoitteena on löytää vaihtoehtoinen menetelmä kerrostumisasteen laskennalle, sillä epätarkkuuksien havaittiin liittyvän siihen.

Menetelmän löytämiseksi suoritettiin lyhyt kirjallisuustutkimus ja lupaava ehdokas uudeksi malliksi löydettiin ja implementoitiin APROS:iin. Uutta mallia testattiin vertailemalla sillä laskettuja tuloksia kahden eri koelaitteiston mittaustuloksiin ja nykyisen version laskentatuloksiin. Tulokset olivat osin ristiriitaisia, joissain tapauksissa uusi laskentamenetelmä oli nykyistä tarkempi, joissain tilanne oli päinvastainen. Yleisesti ottaen uutta menetelmää voi kuitenkin luonnehtia parannukseksi.

ACKNOWLEDGEMENTS

This Master's thesis was written at VTT Technical Research Centre of Finland in the Nuclear Power Plant Modelling Team. I wish to thank the entire organization for the opportunity to complete my Master's degree in such a supportive environment.

I am most grateful to my instructor and examiner Dr. Tech. Markku Hänninen for introducing me to this topic and for his invaluable help and guidance during the entire process. For giving me an opportunity to work on my thesis, my gratitude goes to Dr. Tech. Eija-Karita Puska.

From Lappeenranta University of Technology I would like to thank Prof. Riitta Kyrki-Rajamäki for her role as my examiner, as well as for her inspiring classes that were a significant factor when choosing nuclear engineering as my focus.

Finally, I would like to thank my family and friends for their continuing support and encouragement.

TABLE OF CONTENTS

TABLE OF FIGURES

NOMENCLATURE

A	area	[m^2]
c	two phase friction multiplier	[-]
D	diameter	[m]
E	rate of entrainment	[-]
F	friction force/volume	[N/m^3]
g	gravitational acceleration	[m/s^2]
H	height	[m]
h	height, specific enthalpy	[m], [J/kg]
L	level	[m]
m	mass	[kg]
q	heat flow/volume	[W/m^3]
R	rate of stratification	[-]
t	time	[s]
u	velocity	[m/s]
z	space coordinate	[m]

Greek

α	void fraction	[-]
Γ	mass phase change rate	[kg/m^3s]
Δ	difference	[-]
η	dynamic viscosity	[kg/ms]
θ	angle for liquid level	[°, rad]
ρ	density	[kg/m^3]
σ	surface tension	[N/m]
φ	flow channel inclination	[°, rad]

Subscripts

a	annular
b	bubbly
d	droplet
en	non-stratified with entrainment
g	gas
h	hydraulic
i	interface
k	phase
l	liquid
LM	Lockhart-Martinelli
nc	non-condensable
ne	non-stratified without entrainment
ns	non-stratified
s, st	stratified
w	wall

ABBREVIATIONS

APROS	Advanced Process Simulation Environment
CCFL	Countercurrent Flow Limitation
IVO	Imatran Voima Oy
LOCA	Loss of Coolant Accident
LWR	Light Water Reactor
PWR	Pressurized Water Reactor
RCP	Reactor Coolant Pump
SBLOCA	Small Break Loss of Coolant Accident
SG	Steam Generator
UPTF	Upper Plenum Test Facility
VTT	Technical Research Centre of Finland
VVER	Voda Vodjanyi Energetitseskij Reaktor

1 INTRODUCTION

APROS (Advanced Process Simulation Environment) is a computer simulation program developed to simulate thermal hydraulic processes in nuclear and conventional power plants. It was originally developed by VTT Technical Research Centre of Finland and Imatran Voima Oy (predecessor of Fortum Ltd). It is currently co-owned and co-developed by VTT and Fortum Ltd.

In this thesis the APROS 6-equation model is introduced briefly, with interfacial friction between phases, flow regimes and phase stratification being of special interest. In earlier simulations, current version (5.08) of the six-equation model was found to produce inaccurate results in certain cases of two-phase flow when flow channels were inclined. [Hillberg 2009] To improve the simulation model in these cases, a brief literature study of the subject area was conducted and improvements in calculation methods are introduced and tested. Experimental data was obtained from full-scale loop seal experiments conducted by Imatran Voima Oy [Tuomisto 1988] and Siemens-KWU [Liebert 1998].

2 SIX-EQUATION MODEL OF APROS

To calculate two-phase flow (e.g. liquid water and steam) APROS has several methods from which the user can choose, depending on the needed accuracy level: homogenous model, 5-equation (drift-flux) model, and 6-equation model. In the following chapter, the six-equation model of APROS is briefly introduced, with focus on flow regimes, friction correlations and rate of stratification. [Hänninen 2008]

The 6-equation model is the most sophisticated of the flow models in APROS. It calculates the needed parameters for describing a system with gas and liquid phases, e.g. pressures, void fraction, enthalpies and velocities separately for both phases instead of making assumptions about the nature of the two-phase flow. [Hänninen 2008] This requires more calculation, but it will also describe the process more accurately. Using models which don't calculate both phases separately, such as drift-flux model (or 5-equation model), will always result in loss of flow characteristics. [Ishii, Hibiki 2006] In the current APROS the calculation of non-condensable gases is also possible. The feature is essential in system codes used for analyzing light water reactor (LWR) transients, such as primary circuit leakages. [Hänninen, Ahtinen 2009]

2.1 Governing equations of the six-equation model

In APROS, state variables such as pressure and void fraction are calculated in defined control volumes called nodes. Vector quantities such as velocity are calculated in control volumes between nodes, called branches. Each branch connects two adjacent nodes. This type of control volume arrangement is called a staggered grid.

To calculate the two-phase flow system, APROS uses six partial differential equations - three for both phases – which are based on conservation equations of mass, momentum and energy. If the system includes non-condensable gas, it will need to be calculated separately. The differential equations are presented as follows:

$$\frac{\partial \alpha_k \rho_k}{\partial t} + \frac{\partial \alpha_k \rho_k u_k}{\partial z} = \Gamma_k \tag{1}$$

$$\frac{\partial \alpha_k \rho_k u_k}{\partial t} + \frac{\partial \alpha_k \rho_k u_k^2}{\partial z} + \alpha_k \frac{\partial p}{\partial z} = \Gamma_k u_{ik} + \alpha_k \rho_k \vec{g} + F_{wk} + F_{ik} + f_k(v, pu, fl) \tag{2}$$

$$\frac{\partial \alpha_k \rho_k h_k}{\partial t} + \frac{\partial \alpha_k \rho_k u_k h_k}{\partial z} = \alpha_k \frac{\partial p}{\partial t} + \Gamma_k h_{ik} + q_{ik} + q_{wk} + F_{ik} u_{ik} + \alpha_k \rho_k u_k \vec{g} \tag{3}$$

$$\frac{\partial (\alpha_g \rho_{nc})}{\partial t} + \frac{\partial (\alpha_g \rho_{nc} u_g)}{\partial z} = 0 \tag{4}$$

Equation (1) describes the conservation of mass, equation (2) the conservation of momentum, equation (3) the conservation of energy and equation (4) the mass conservation for the non-condensable gas. Subscript *k* refers to either gas or liquid phase, *i* refers to the interface of the phases and *w* refers to the wall of a flow channel. In equation (2) the function f_k describes the valves, pumps and form loss coefficients to take any obstacles in the flow channel into account. The calculation of wall friction F_w, interfacial friction F_i, interfacial heat transfer q_i and wall heat transfer q_w is based on empirical correlations which have a significant effect on the solution. Empirical correlations are required to couple together the quantities solved with the six partial differential equations. To solve the equations (1) to (4) numerically, they must first be discretized in respect to time and space and the non-linear terms must be linearized. Full discretization is presented in reference [Hänninen 2008] and won't be shown here, as it's not relevant to this thesis. The main area of interest in this thesis is the interfacial friction F_i used in equations (2) and (3).

2.2 Flow regimes

Two-phase flow can have several different flow types, depending on the flow conditions, such as velocity, void fraction, channel dimensions, channel inclination, etc. Caused by surface tension and interfacial friction between the two phases, phases tend to fill the flow

channel in very distinct manner in a given flow scenario. These types are usually called flow regimes or patterns, and they are of major importance when simulating two-phase flow numerically, because the nature of each flow type differs from the others significantly. Typical flow regimes in vertical flow channels are presented in Figure 1.

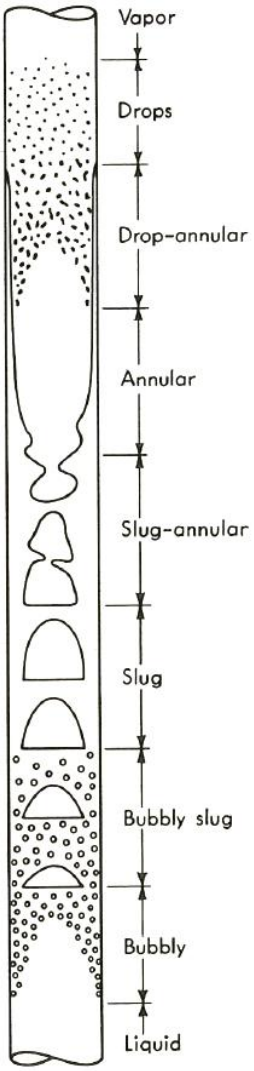

Figure 1. Typical flow regimes in a vertical flow channel. [Wallis 1969]

Flow regimes in horizontal flow channel differ slightly from the ones in a vertical channel, as seen in Figure 2. In a horizontal flow channel, the two phases are much less symmetrically distributed along the cross-section of the flow channel due to density difference of the phases.

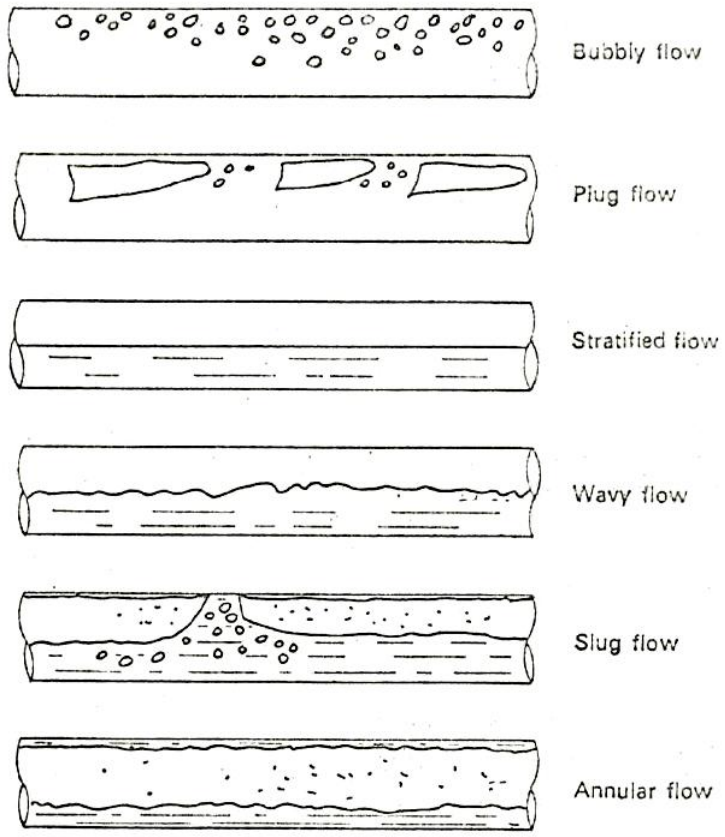

Figure 2. Typical flow regimes in a horizontal flow channel. [Hewitt, Hall-Taylor 1970]

Although flow regimes are visually identifiable, a method for concluding the current flow regime without visual contact is needed. It is often impossible or unpractical to set visual monitors in flow channels. Because of the irregular and unstable nature of the flow regimes and the transitions between them, analytical treatment of the flow regime calculation is challenging. Therefore the different flow regimes are taken into account via empirical correlations which have been developed through experimentation and measurements in different conditions.

The empirical correlations used to describe friction and heat transfer between gas and liquid phases as well as between flow channel walls and both phases depend heavily on the flow regime. Usually different correlations are used for different flow regimes and the common scenario where the prevailing flow regime is not a distinct regime but a combination of several flow types, the different correlations are used with weighting

coefficients. Coefficients used in APROS are the rate of stratification, the rate of entrainment and the void fraction. The flow regimes used in APROS are bubbly, annular, droplet and stratified flows. [Hänninen 2008]

2.3 Friction correlations

Wall and interface friction correlations are an important part of additional equations which are needed to close the system formed by six partial differential equations. Friction is calculated for the interface between liquid and gas phases and between both phases and the channel wall. In this chapter those correlations are discussed with relation to the rate of stratification, the main focus of the thesis. Therefore the equations for every friction factor correlation are not presented, only the ones where rate of stratification is used.

2.3.1 Wall friction

For calculating wall friction, APROS first calculates the friction factor for both phases separately. User can choose whether correlations are for smooth or rough pipes. For laminar flows, friction factor in a round pipe can be deduced analytically, but for turbulent flow or for flow channels with non-circular cross section experimental correlations are needed. To define whether the flow is laminar or turbulent, the Reynolds number is calculated. For turbulent flow in smooth pipes the Blausius correlation is used, and Colebrook equation is used for rough pipes.

Two phase friction multiplier is used to calculate pressure drop in two phase flow and to estimate phase distribution on the flow channel. The multiplier depends on the flow regime: it's defined separately for stratified flow, non-stratified flow without droplet entrainment and non-stratified flow with droplet entrainment. Two phase friction multipliers for gas and liquid phases are defined as

$$c_g = Rc_{g,st} + (1-R)c_{g,ns}, \tag{5}$$

$$c_l = Rc_{l,st} + (1-R)\{(1-E)c_{l,ne} + Ec_{l,en}\}, \tag{6}$$

where E is the rate of entrainment, subscript *st* stratified flow, *ns* non-stratified flow, *ne* non-stratified flow without entrainment and *en* non-stratified flow with entrainment. For stratified flow the multiplier $c_{k,st}$ is the perimeter of the flow channel occupied by the phase in question. The flow channel is assumed to be circular. Multipliers for stratified flow are defined as

$$c_{g,st} = \frac{2\theta}{2\pi} = \frac{\arccos\left(\frac{2L_l}{H} - 1\right)}{\pi}, \tag{7}$$

$$c_{l,st} = 1 - c_{g,st} \tag{8}$$

In equation (7) L_l is the liquid level in the channel, H channel height, i.e. diameter for horizontal pipe, and θ the angle between a vertical line and a line drawn from the channel centre to the intersection of the channel perimeter and the liquid level. Illustration of the geometrical properties is shown in Figure 3, numbers 1 and 2 stand for gas and liquid phases.

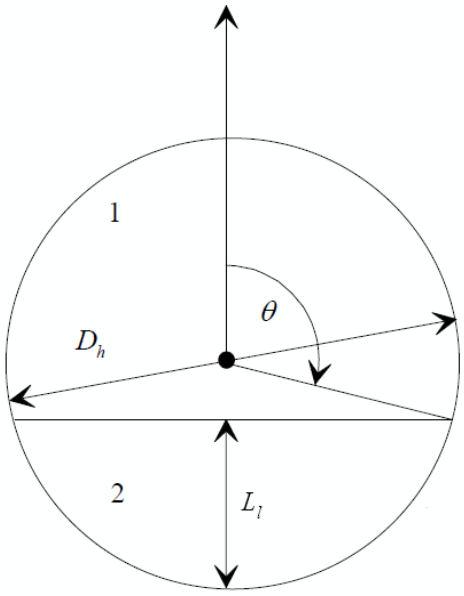

Figure 3. Definition of the geometrical characteristics for stratified flow.

If the flow is not stratified and void fraction and entrainment are relatively low, only liquid phase touches the channel wall. Multiplier for non-stratified gas flow is defined as

$$c_{g,ns} = \alpha^{1.25}. \tag{9}$$

Mass fraction of the liquid is used as the multiplier for non-stratified liquid flow without entrainment, and is defined as

$$c_{l,ne} = X_l = \frac{(1-\alpha)\rho_l}{\alpha\rho_g + (1-\alpha)\rho_l}. \tag{10}$$

In the case of non-stratified liquid flow with entrainment, modified Lockhart-Martinelli model is used. The multiplier is defined as

$$X_{LM} = \sqrt{\frac{\rho_g}{\rho_l}}\left(\frac{\eta_l}{\eta_g}\right)^{0.1}\left(\frac{m_l}{m_g}\right)^{0.9} \tag{11}$$

$$c_{l,en} = \left(1 + \frac{20}{X_{LM}} + \frac{1}{X_{LM}^2}\right) f(\alpha) \tag{12}$$

Definition for the Lockhart-Martinelli parameter in equation (11) applies for a case when both phases are in turbulent flow, but according to Lockhart & Martinelli [Lockhart, Martinelli 1949], the formulas for other flow regimes do not differ significantly from the model used in APROS. [Hänninen, Ylijoki 2005] The model used is compared with experimental data from several sources, and it was found to agree quite well on low pressures (< 2 MPa), but it overestimates wall friction slightly on higher pressures. [Bestion 1990b]

2.3.2 Interfacial friction

The friction between gas and liquid phases, the interfacial friction, depends strongly on the prevailing flow regime. Therefore different flow regimes require different correlations for

the friction calculation. APROS has correlations for stratified and non-stratified flow, which consists of bubbly, annular and droplet flow. Interfacial friction is then obtained as a weighted average of the different correlations, with void fraction, rate of stratification and rate of entrainment as weighting coefficients. Final interfacial friction is defined as

$$F_i = RF_{is} + (1-R)\{(1-E)\left[(1-\alpha)F_{ib} + \alpha F_{ia}\right] + EF_{id}\}, \tag{13}$$

where subscript *i* denotes the interface between gas and liquid, *s* stratified flow, *b* bubbly flow, *a* annular flow and *d* droplet flow. Momentum conservation equations are coupled with the following definition:

$$F_i = F_{il} = -F_{ig}\,. \tag{14}$$

APROS has different friction correlations not only for different flow regimes, but for different flow channel geometries as well. Calculation of interfacial friction for bubbly flow can be selected from five alternatives, of which one simulates pipe geometry, and other four are used in rod bundle geometries. These are most commonly used for calculating the flow in reactor core or the secondary side of a vertical steam generator in a PWR. Different alternatives are based on countercurrent flow limitation (CCFL) correlations. As the individual correlations for the interfacial friction for different flow regimes or channel geometries do not contain the rate of stratification, they are not very relevant in the scope of this thesis. Therefore, they are not shown here. Correlations used are well tested against experimental results, and are in good agreement. However, typical experiments are done in small scale, so their applicability to full-scale simulations is not guaranteed. [Hänninen, Ylijoki 2005]

2.4 Rate of stratification

Rate of stratification is one of the weighting coefficients to ensure smooth transition between correlations for different flow regimes, and it describes the separation rate of the two phases. If the rate of stratification is 1, flow is fully stratified, e.g. gas and liquid phases are completely separated. If the rate of stratification is 0, phases are completely

mixed. All values between 0 and 1 are also possible, and then phases are mixed to some degree. The rate of stratification in APROS is defined as

$$R = R_1 R_2 , \tag{15}$$

where R_1 comes from the Kelvin-Helmholtz stability criterion and R_2 describes phase mixing due to liquid turbulence. In [Wallis 1969] Kelvin-Helmholtz stability criterion is written as

$$\left(u_g - u_l\right)^2 > (\rho_l - \rho_g) g D_h \left(\frac{\alpha}{\rho_g} + \frac{1-\alpha}{\rho_l} \right), \tag{16}$$

where g is the gravitational acceleration and D_h the hydraulic diameter of the flow channel. This criterion can also be written as

$$\frac{\left(u_g - u_l\right)^2 \rho_g \rho_l}{\alpha\rho_l + (1-\alpha)\rho_g} > (\rho_l - \rho_g) g D_h \tag{17}$$

which is the form implemented into APROS with some modifications made for numerical reasons. First, both sides of equation (17) are multiplied by $\alpha(1-\alpha)$ to remove stratification when void fraction is either very high (gas flow) or very low (liquid flow). Secondly, a low limit of 10^{-8} m/s is given for the minimum velocity difference of the phases. Finally, the gravitational component perpendicular to the flow direction (g_1) is used instead of the constant gravitational acceleration (this is used as a simple method to take channel inclination into consideration) and even this component is limited so that for channel inclinations above 60 degrees stratification is not allowed. Both sides of the resulting equation are defined separately, as

$$P_{ins} = \frac{\alpha(1-\alpha)\rho_g \rho_l}{\alpha\rho_l + (1-\alpha)\rho_g} Max(|u_g - u_l|^2, 10^{-8}) + 10^{-2}(\rho_l - \rho_g) g_1 D_h \tag{18}$$

and

$$P_{is} = \alpha(1-\alpha)(\rho_l - \rho_g)g_1 D_h . \tag{19}$$

P_{ins} describes how the flow tries to disintegrate into mixed flow, due to instability of the interface. P_{is} describes the pressure difference between the interface and the average pressure in stratified flow, which makes stratified flow conditions more stable. It is therefore logical to describe the rate of stratification as a ratio of the mixing and stabilizing forces:

$$X = \frac{P_{ins}}{P_{is}} . \tag{20}$$

In essence, X is the ratio of the forces that destabilize and stabilize the flow. If the destabilizing forces are larger, stratified flow becomes unstable and changes into intermittent flow. R_1 used in equation (15) is defined as

$$\begin{aligned} &X < 0.25 \rightarrow R_1 = 1 \\ &0.25 \le X \le 1 \rightarrow R_1 = \frac{2}{0.75^2}\left(X-1\right)^2\left(X-0.125\right) \\ &X > 1 \rightarrow R_1 = 0 \end{aligned} \tag{21}$$

The low limit for X is an experimental threshold for onset of instabilities, while high limit is the theoretical threshold above which no stratified flow can exist. Between the limits the value for R_1 is interpolated to describe a flow where phases are somewhat mixed [Bestion 1990a]

R_2 in equation (15) is defined as

$$\begin{aligned} &u^* < 40 \rightarrow R_2 = 1 \\ &40 \le u^* \le 90 \rightarrow R_2 = \frac{1}{50^3}\left(u^*-90\right)^2\left(2u^*-30\right) \\ &90 < u^* \rightarrow R_2 = 0 \end{aligned} \tag{22}$$

where

$$u^* = |u_l| \left(\frac{\sigma g \Delta \rho}{\rho_l^2} \right)^{-0.25} , \tag{23}$$

which represents the ratio of turbulence mixing forces to buoyancy stratifying forces in mixed flow. Limits in equation (22) are based on experimental studies performed on SUPER MOBY DICK loop facility. [Bestion 1990b] [Bestion 1990a]

2.5 Rate of entrainment

The rate of entrainment is another weighting coefficient used to calculate two-phase friction. It defines the fraction of liquid phase which exists in droplets. This is significant to interfacial friction calculation, since the surface area of the interface increases as more droplets are present in the flow. The rate of entrainment is defined in APROS as

$$E = \left(\frac{1.8 \cdot 10^{-4} \sigma}{\alpha |u_g| \eta_g} \sqrt{\frac{\rho_l}{\rho_g}} \right)^2 \cdot f(\alpha) , \tag{24}$$

where function *f* restricts the droplet flow in low void fractions. For void fractions under 0.5 the rate of entrainment is 0, and for $\alpha > 0.75$ the function $f(\alpha) = 1$. Equation (24) approximates the experimental data given in [Wallis 1968]. Values for the rate of entrainment given by equation (24) are in good agreement with experimental results for pressure range of 0.1 – 0.4 MPa and gas velocities between 6 and 75 m/s. [Hänninen, Ylijoki 2005]

3 NEW METHOD FOR THE RATE OF STRATIFICATION

To improve the simulation model, an alternative method for calculating the rate of stratification was needed. A brief literature research was conducted, and a promising candidate for the new method was found and implemented in the simulation code. The new method is described in this chapter.

During the literature research it soon became clear that Kelvin-Helmholtz stability criterion is at least partly used in many simulation models aimed at calculating the conditions in which stratified two-phase flow can occur. The current model in APROS is also partly based on this method. The alternative method introduced in this project is also based on the same stability criterion, but the implementation is somewhat different than the current model and leads to significant difference in simulation results. The method introduced here is presented in more detail in reference [Kolev 2007].

To explain the background of the new method, we'll start with the basic form of the Kelvin-Helmholtz stability criterion, which can be written as

$$u_{g,stratified} - u_l = \left[g\cos(\varphi - \frac{\pi}{2})(\rho_l - \rho_g)\left(\frac{\alpha_g}{\rho_g} + \frac{1-\alpha_g}{\rho_l}\right) \Big/ \frac{d\alpha_l}{dL_l} \right]^{1/2}, \qquad (25)$$

where φ is the angle between upwards oriented vertical line and flow channel axis (see Figure 4 for an illustration). Equation (25) gives the limit for the velocity difference between phases in stratified flow. If the difference becomes larger, stratified conditions are no longer possible and flow disintegrates into intermittent flow.

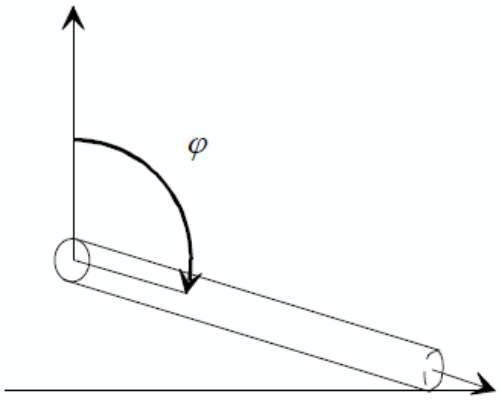

Figure 4. Illustration of the angle for flow channel inclination. [Kolev 2007]

The general form of the stability criterion can be applied to any flow channel cross section, but as the circular cross section is most commonly needed, defining the criterion for pipe geometry is useful. To do that, we need to define the derivative term in equation (25). For circular cross section the relation between liquid volume fraction and liquid level can be written as

$$1-\alpha_l = \frac{\theta - \sin\theta\cos\theta}{\pi}, \tag{26}$$

where θ is the angle between a vertical line and a line drawn from the channel centre to the intersection of the channel perimeter and the liquid level (see Figure 3). Liquid level can be given as a function of this angle:

$$L_l = \frac{1}{2} D_h (1+\cos\theta). \tag{27}$$

Now the derivative term in equation (25) can be written as

$$\frac{d\alpha_l}{dL_l} = \frac{d\alpha_l}{d\theta} \Big/ \frac{dL_l}{d\theta} = \frac{4}{D_h}\frac{\sin\theta}{\pi}. \tag{28}$$

This form of the criterion has been compared with experimental results, and it was found that it is not very accurate on large diameter pipes. A constant multiplier of 0.5 was introduced when the criterion was compared to experimental results from flow channels with diameter ranging from 0.0254 to 0.305 m [Wallis, Dodson 1973] A constant multiplier of 0.487 was later suggested when low pressures were considered. [Mishima, Ishii 1980] Obviously, a multiplier of some kind is necessary, but as the constant multipliers are only confirmed on specific test cases, a more versatile option would be preferable.

As a slightly more analytical alternative to the constant multipliers shown earlier, $(1-L_l D_h^{-1})$ was nominated as the criterion [Taitel, Dukler 1976]. This multiplier has also been compared against experimental results performed on relatively large diameter pipes (0.18 m) and high pressures (3 – 7.3 MPa) [Anoda et al. 1989] and it's validity was confirmed. This form of the multiplier can be given as a function of θ using equation (27). Adding this multiplier and the definition from equation (28) to the basic criterion in equation (25) we obtain

$$u_{g,stratified} - u_l = \frac{1}{2}(1-\cos\theta)\left[\frac{g\cos(\varphi-\frac{\pi}{2})(\rho_l-\rho_g)}{\frac{4}{D_h}\frac{\sin\theta}{\pi}}\left(\frac{\alpha_g}{\rho_g}+\frac{1-\alpha_g}{\rho_l}\right)\right]^{1/2} \tag{29}$$

which is the new criterion implemented into APROS. In essence, when the velocity difference between phases exceeds the limit given by the right hand side of equation (29), stratified flow conditions are no longer possible, and rate of stratification is zero. To keep the changes as compact as possible, the new criterion is used in APROS in the following form:

$$X = \frac{u_{g,stratified} - u_l}{\frac{1}{2}(1-\cos\theta)\left[\frac{g\cos(\varphi-\frac{\pi}{2})(\rho_l-\rho_g)}{\frac{4}{D_h}\frac{\sin\theta}{\pi}}\left(\frac{\alpha_g}{\rho_g}+\frac{1-\alpha_g}{\rho_l}\right)\right]^{1/2}}, \tag{30}$$

which is similar to the expression used in the current model (equations 20 & 21). It was decided that the low limit for the interpolation (equation 21) would not be changed. As can be seen, the new model only affects the calculation of R_1 in equation (15). R_2 is calculated as before.

Before doing the final modifications in the source code, some initial comparisons between the calculation methods were done to see whether they give different results for the rate of stratification or not. The variables in equation (30) were recorded during the simulations and the rate of stratification was manually calculated and compared to the values achieved with the current method. Comparisons were made using simulations of the IVO loop seal experiments (introduced in chapter 5) with mid-range air flow speed (5 m/s). It was found that the difference was notable.

The actual implementation was a fairly straightforward process, as most of the variables in equation (30) were already included in APROS source code in one form or another. The angle θ, which represents the liquid level in the calculation node was calculated from the equation (27), since APROS already has its own subroutine for calculating the liquid level as a function of void fraction. The criterion was written in FORTRAN using the existing subroutines for calculating the rate of stratification as a basis. Modifying the current source code was done with as few changes as possible to prevent any unintentional changes in other simulation cases.

4 LOOP SEALS

In a pressurized water reactor (PWR) the loop seals between steam generators (SG) and reactor coolant pumps (RCP) may significantly affect the reactor core water level depression and core temperature during a cold leg loss-of-coolant accident (LOCA). Before the steam generated in the core is able to push water out of the loop seal - thus clearing it - a considerable pressure difference will be created, lowering the water level in the reactor core. In the following chapter, loop seal behaviour is briefly described.

4.1 Formation of a loop seal

During normal operation, the primary circuit of a PWR is kept in a pressure where water remains as liquid. However, in a loss-of-coolant accident (LOCA) the pressure will drop, causing the coolant to boil, which creates two-phase flow conditions in the primary circuit. The steam flowing from the reactor pressure vessel condenses into liquid in the steam generator, and may flow down into U-shaped pipe bends and fill them. If the pipe bend is completely filled with water, steam flow in the circuit might be prevented, and cooling of the reactor core is jeopardized.

Formation of the loop seal requires that a U-shaped pipe bend exists somewhere in the circuit. In a typical PWR, the loop seal is formed in the cold leg, as the reactor coolant pump has a vertical axis, which requires the pipe bend to operate. Typical cold leg loop seal is shown in Figure 5.

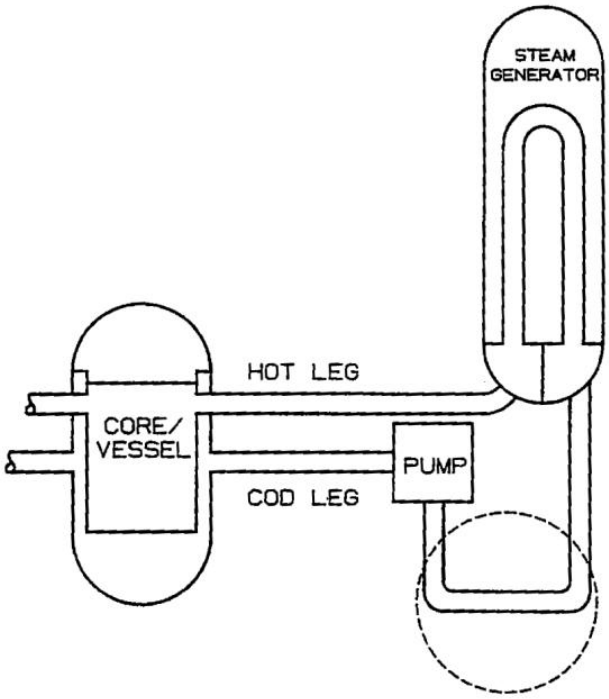

Figure 5. Cold leg loop seal in a typical Western PWR. [Lee et al. 1983]

Cold leg loop seal is present in nearly all Western and Russian PWR-designs.

Depending on the placement of the steam generators, loop seal can also be formed in the hot leg. If the steam generator is not high enough compared to the pressure vessel, a U-shaped pipe bend is also needed in the hot leg, as seen in Figure 6.

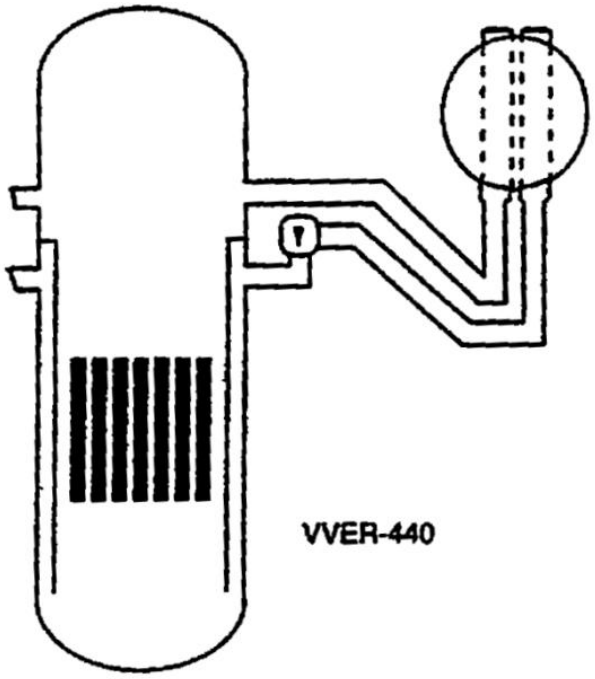

Figure 6. Loop seals in the primary circuit of a VVER-440. [Haapalehto 1995]

An example of such a design is the Russian VVER-440. [Ohvo 1998]

4.2 Effect of loop seals in the primary circuit

In LOCA situations the water level in reactor core depends on various pressure loss mechanisms in the primary circuit, when steam flows from the core to the break. Loop seals between RCP and SG can have a significant effect on the total pressure loss in the system. Pressure loss in the loop seal is a combination of different two-phase flow mechanisms in the horizontal loop seal pipe, vertical pipe to the RCP and the RCP itself. The hydraulic head in the vertical pipes is also a significant factor. The flow regime has a notable effect on the pressure loss. During SBLOCA (small break loss of coolant accident), the flow regime in the horizontal pipe section of the loop seal can be stratified, slug or annular flow. Additionally, steam flow can push the water from the loop seal to the vertical pipe leading to the RCP causing a sizeable pressure loss. Stopped RCP also causes a flow resistance which has a factor in the total pressure loss.

When the pressure difference over the loop seals increases, water moves from the reactor core towards the cold leg through the downcomer, and the water level in the core

decreases. Water level may drop as low as the horizontal section of the loop seal, which in a typical PWR is below the core. As a result, reactor core may be briefly exposed before the steam in the primary circuit clears the loop seal and pushes the water back from the downcomer into the core. Loop seal clearing is shown in Figure 7.

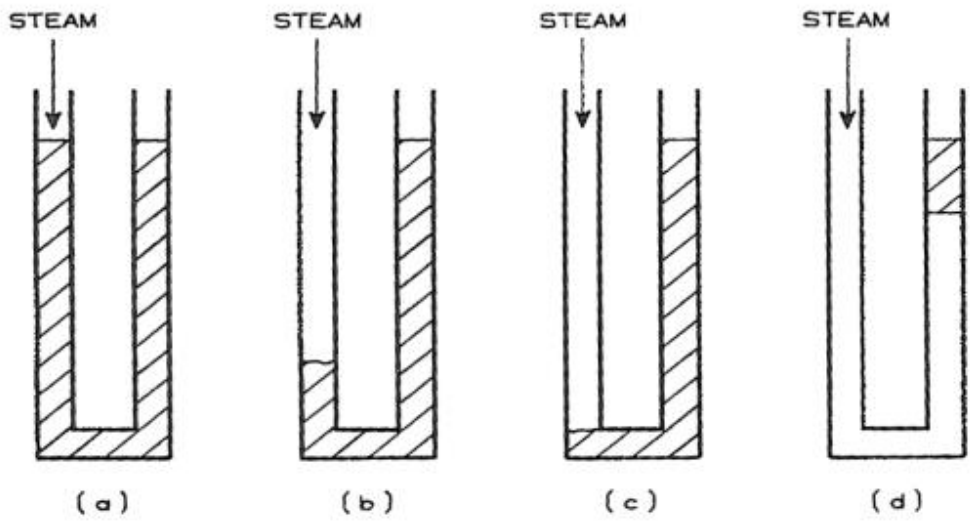

Figure 7. Phases of loop seal clearing. [Lee 1987]

In phase a) steam flow through the loop seal is blocked. Water level starts to decrease in phase b) when steam flow pushes water to the RCP side. In phase c) the loop seal is nearly cleared, as the steam reaches the horizontal pipe, and in phase d) steam has cleared the loop seal. After loop seal has been cleared, pressure in the core drops suddenly, and steam pushes water from the cleared loop to the downcomer and the reactor core, and possibly to other loops. This reverses the flow direction temporarily, and if the reversed flow is not strong enough, the water is not pushed through the SG, and flows back to the bottom of the loop seal when flow direction returns to normal. This causes fluctuations in the water levels in the reactor core and the loop seal. Loop seal behaviour is strongly dependent of the break size.

The effect of loop seals is especially significant in plants which have loop seals in both hot and cold legs of the primary circuit – such as the VVER-440 (e.g. Loviisa 1 & 2). Up to 8

% of the total water inventory of the primary circuit can be in loop seals, and the effect on water level in the reactor core is even more significant. A filled loop seal in the hot leg can also prevent natural circulation of the coolant, and stop heat transfer from the core. [Ohvo 1998]

5 TEST FACILITIES AND EXPERIMENTS

When developing simulation models and calculation methods for system codes such as APROS, extensive and reliable experimental data is of utmost importance. Facilities which provided the experimental results for this project are introduced in this chapter.

5.1 IVO Loop seal facility

To accurately analyse PWR accidents with thermal-hydraulic simulation codes, such as APROS, correct modelling of loop seal clearing is required. For this purpose, Imatran Voima Oy (IVO) has performed loop seal experiments in a full scale facility, which corresponds to the geometry of a cold leg loop seal in a VVER-1000 PWR. Schematic of the loop seal facility is shown in Figure 8.

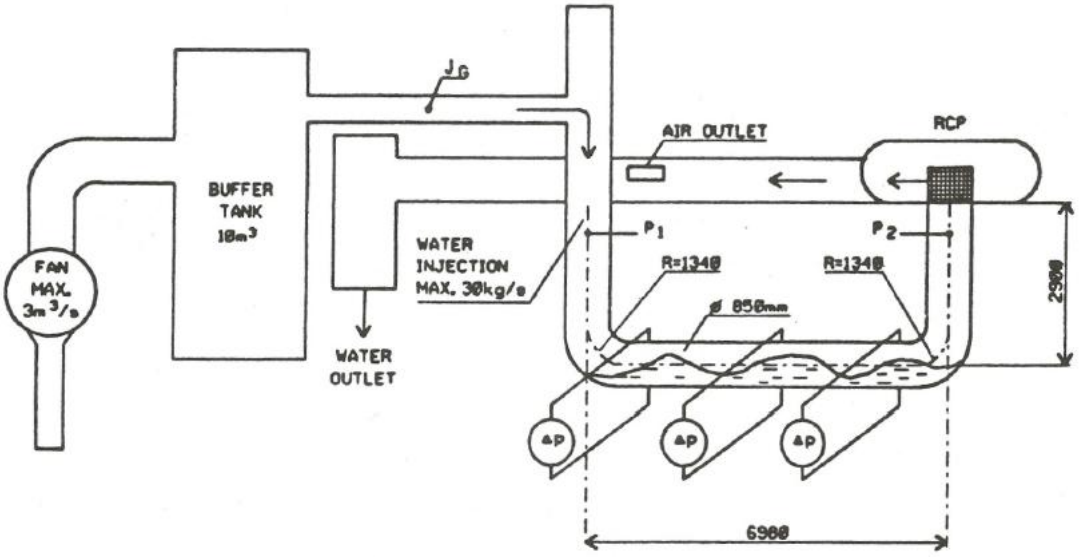

Figure 8. IVO Loop Seal Facility. [Kymäläinen 1992]

To simulate the steam flow during a LOCA, the facility has a high-capacity fan which is capable of providing air into the loop seal up to the superficial velocity of 9 m/s. To dampen oscillations in the air flow during an experiment, the facility has a 10 m^3 buffer tank. The actual loop seal itself has an inner diameter of 850 mm and is connected to a

mock-up of a reactor coolant pump (RCP), which has the single phase pressure drop and the over-flow edge of an actual RCP.

All experiments were conducted under atmospheric pressure and at room temperature. Initial water level in the loop seal and superficial air velocity in the inlet were used as test parameters. In addition to inlet air velocity, pressure was measured in several areas of the facility, with pressure difference over the loop seal being of special interest. Possible changes in the flow regime during the experiments were observed visually through windows in the horizontal pipe. After each experiment, residual water level in the facility was measured. [Kymäläinen 1992]

5.2 Upper plenum test facility (UPTF)

The Upper Plenum Test Facility (UPTF) is a full-scale simulation facility of the primary system of a 1300-MW PWR from Siemens-KWU. It was also constructed and operated by the same company. The facility simulates the test vessel, including original internals, the downcomer and all four connected loops of the real power plant in 1:1 scale. An overall view of the facility is shown in Figure 9. Since the facility has multiple loops, it can simulate the integral behaviour and the sequence of loop seal clearance during a cold leg break, as well as the residual water levels, flow patterns and pressure drops across a single loop seal. As opposed to the IVO Loop Seal facility, which uses air-water configuration in the experiments, UPTF is capable of performing steam-water tests, where steam is injected into the water-filled system. It also has a maximum operating pressure of 20 bar, where the IVO facility conducts their tests in atmospheric pressure.

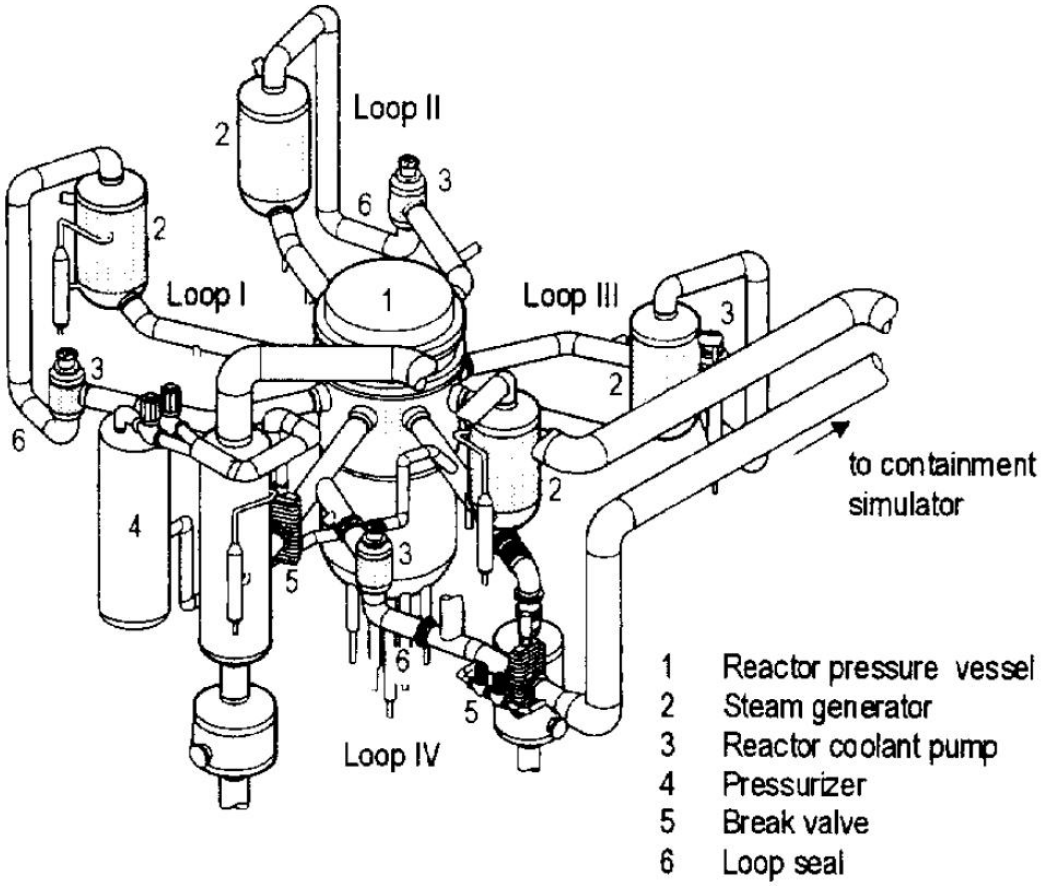

Figure 9. Overall view of the UPTF test facility. [Liebert 1998]

A single loop seal configuration and related instrumentation is presented in Figure 10.

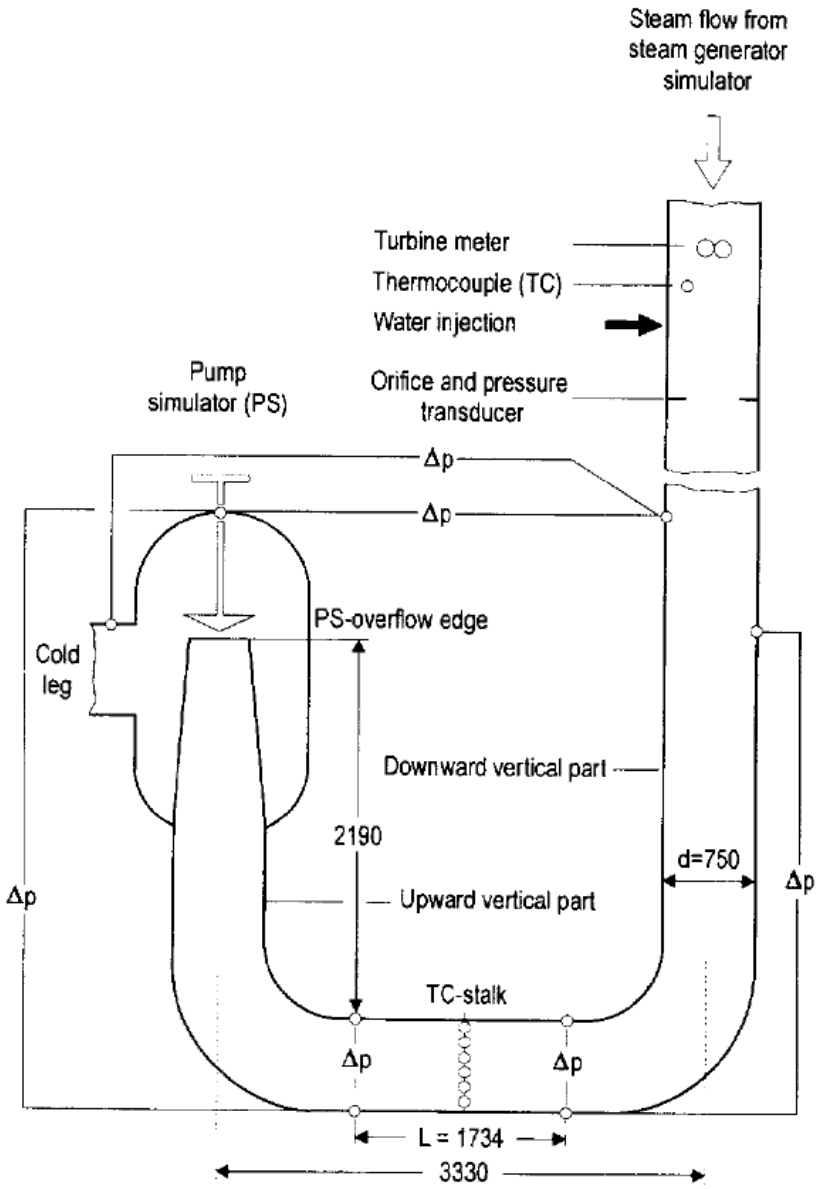

Figure 10. Single loop seal and related instrumentation of the UPTF. [Liebert 1998]

The loop seal consists of a downward vertical pipe, upward vertical pipe, a pump simulator, two 90 degree bends and a horizontal pipe connecting the bends. All pipe components have an internal diameter of 750 mm. The pump simulator is essentially a valve, which simulates the flow resistance of an actual coolant pump. The downward pipe is connected to the steam generator simulator. It also has a turbine meter, thermocouple and pressure measurements to measure the state and velocity of the steam injected into the system. Additional pressure measurements are located in the horizontal pipe, as well as after the pump simulator. Water level measurement is also based on differential pressure. [Liebert 1998]

6 SIMULATIONS WITH THE CURRENT APROS

In earlier simulations of the loop-seal clearing done at VTT, current version of APROS was found to give slightly inaccurate results when compared to the data obtained from IVO loop-seal experiments. [Hillberg, Hänninen 2010] During the project of which this thesis is a part of, similar issues were found with experimental results from UPTF. In this chapter the simulations with the current version of APROS are presented and compared to the experiments.

6.1 IVO Loop Seal Facility

Results obtained from IVO Loop seal facility have been used to test APROS versions for a long time. In earlier simulations (10-15 years ago) the calculation of non-condensable gases was not yet implemented, and the experiment was modelled as a steam-water –case. Current APROS can calculate the air flow in the system.

For simulating the loop seal experiments with the current version of APROS, the test facility was modelled with different degrees of geometric accuracy, i.e. the amount of calculation nodes used to model pipe bends of the flow channel was varied between one and three. The APROS model used for the abrupt 90° corner simulations is presented in Figure 11.

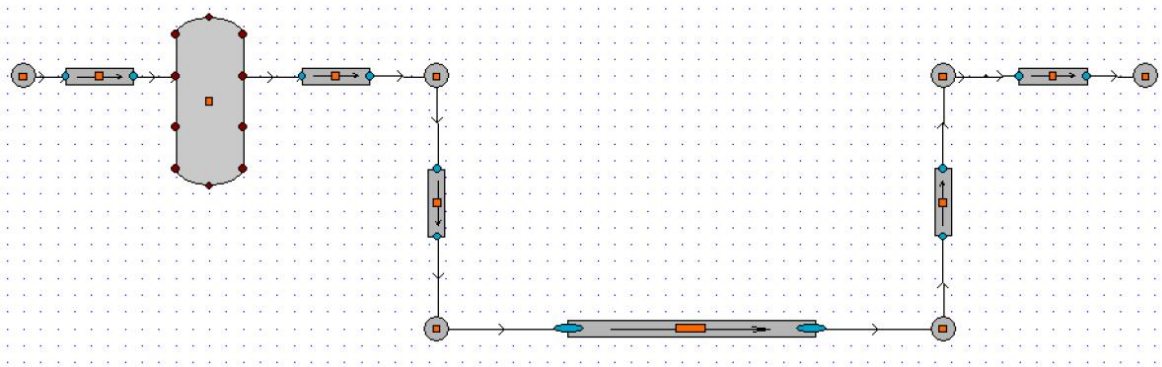

Figure 11. APROS model for the IVO loop seal with 90° corner. [Hillberg 2009]

The APROS model with 90 degree bend was modelled with a buffer tank, as it was found to stabilize the air flow during the simulation. The horizontal pipe was divided into six

calculation nodes. The APROS model for the IVO loop seal facility with three corner nodes is presented in Figure 12. This was the most accurate model used, and it did not require the buffer tank for air flow stabilization. As the horizontal pipe is now shorter, it is now divided into four calculation nodes. [Hillberg 2009]

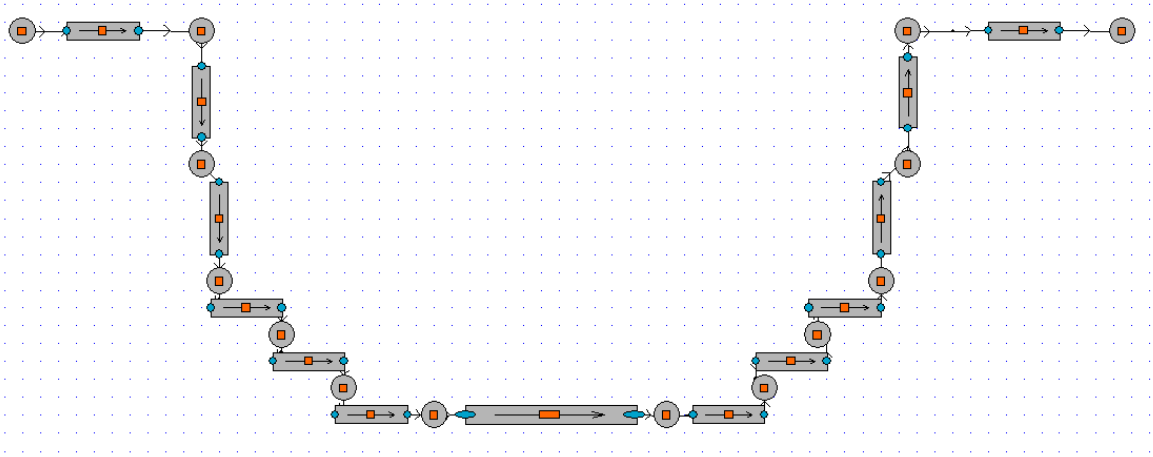

Figure 12. APROS model for the IVO loop seal with 3 corner nodes. [Hillberg 2009]

When the bend was modelled using a single node, as a 90 degree abrupt corner, current APROS gave very good results when compared to experiments. Especially the residual water level in the loop seal was predicted well, as seen in Figure 13, where the residual water level is presented as a function of the superficial air velocity used in the experiment. However, when the amount of corner nodes was increased, and the model was made more accurate geometrically, APROS underestimated the amount of water cleared from the loop seal, thus giving higher residual water levels than the experiments. This is also shown in Figure 13. [Hillberg 2009]

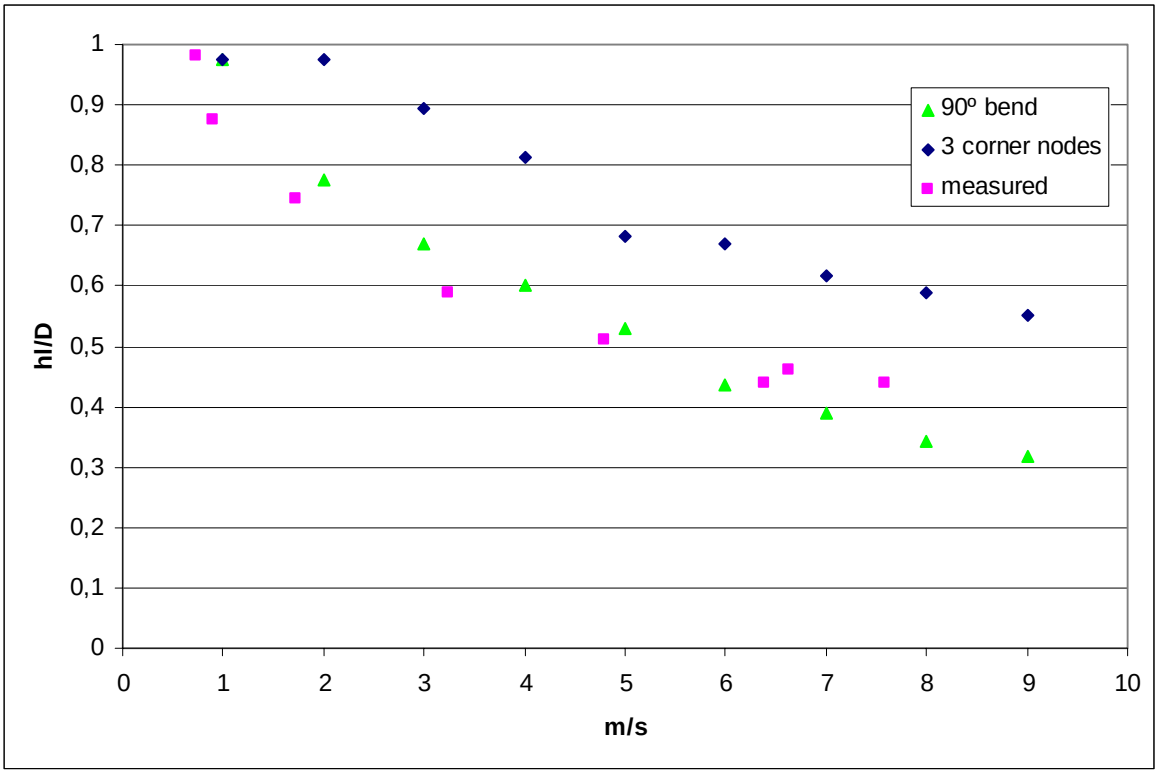

Figure 13. Residual water level in IVO simulations with unmodified APROS. [Hillberg, Hänninen 2010]

Further research suggested that the problem could be related to the manner in which APROS calculates the rate of stratification in inclined flow channels. By limiting the channel angle in which stratified flow is allowed, residual water levels were decreased significantly. Residual water level of these simulations is shown in Figure 14. Two modifications were made in the calculation code. In the first modification (labelled MOD1), rate of stratification is set to zero when channel angle exceeded 17 degrees, which meant that stratified flow was not possible in any of the corner nodes. Residual water levels are now lower than with unmodified APROS, but also lower than was measured during experiments. In the second modification (labelled MOD2), rate of stratification is set to zero when channel angle exceeds 30 degrees. Now stratified flow is allowed in one of the three corned nodes. Residual water levels with this modification were higher than with the first modification, but underestimated the water level when compared to measurements. [Hillberg, Hänninen 2010]

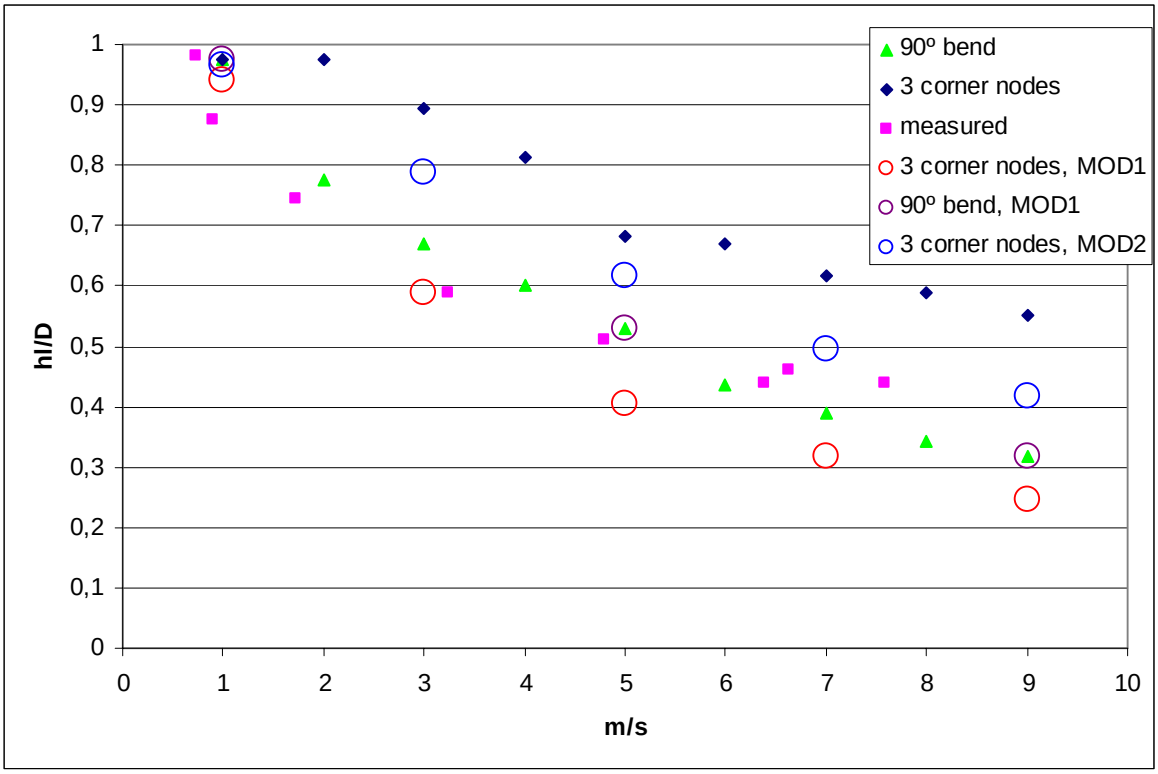

Figure 14. Residual water level in IVO simulations with initial modifications. [Hillberg, Hänninen 2010]

6.2 UPTF

The current version of APROS was also tested with the simulation model of the UPTF. The simulation model used is presented in Figure 15. Due to the similar nature of the test facilities, modifying the IVO loop seal model to match the geometry of UPTF was simple. In addition to the different pipe diameter and lengths, a valve component was added as the pump simulator. Values for the cross-section area and flow resistance matched those found in a real coolant pump. [Liebert 1998] UPTF was only modelled with a three corner node version.

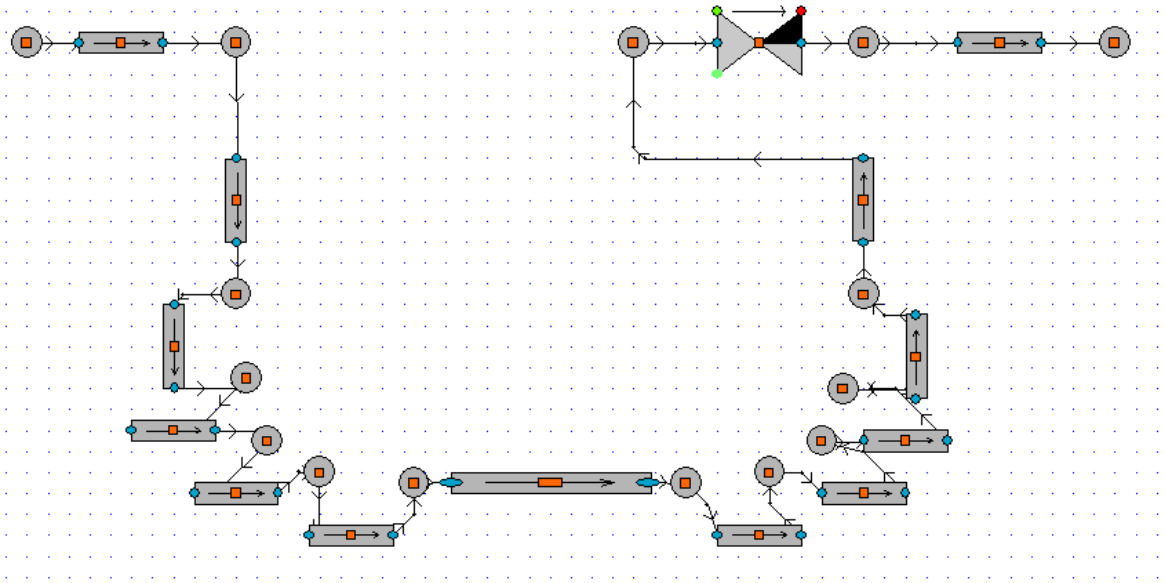

Figure 15. APROS model for the UPTF with three corner nodes.

Again, the residual water level after the experiment was the main interest. The residual water level is shown as a function of Wallis parameter J^*_s in Figure 16. Wallis parameter is defined in equation (31).

$$J_s^* = \frac{\dot{M}_g}{A\rho_g}\frac{\rho_g^{1/2}}{\left[gd\left(\rho_l - \rho_g\right)\right]^{1/2}} \tag{31}$$

Wallis parameter was found to be the most appropriate dimensionless number to make sure pressure scaling would be done accurately considering phenomena like water entrainment, flow pattern, counter-current flow and break flow. Pressure scaling in UPTF experiments is estimated by:

$$J^*_{s,UPTF}(15\,bar) = J^*_{s,PWR}(80\,bar) \tag{32}$$

This estimation was used to define steam mass flow used in the experiments, as well as the break flow area. [Liebert 1998]

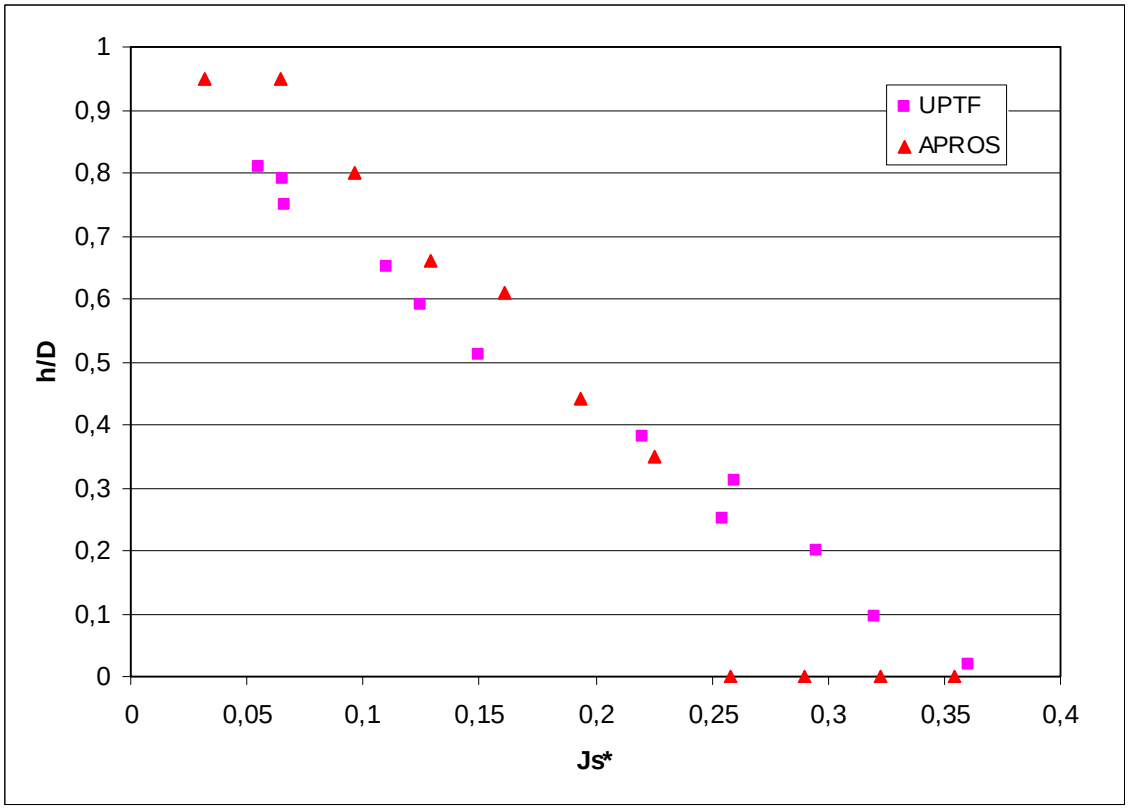

Figure 16. Residual water level in the UPTF experiments and simulations.

The current version of APROS has difficulties predicting the residual water level across the whole test range. With low values of the Wallis parameter (low steam mass flow) the simulation underestimates the water clearance from the loop seal, and the residual water level remains too high. When the Wallis parameter is increased enough (steam mass flow increased) APROS clears the entire loop seal of water, while the experiments show that the residual water level decreases in a linear fashion as steam mass flow increases.

6.3 Conclusions from the simulations

The current version of APROS has difficulties in estimating the residual water level during loop seal clearing. This may result in inaccurate calculation of a loss-of-coolant accident simulation or some other test case where the interfacial friction between phases is relevant. The need for additional development is well justified.

Implemented modifications to the calculation code show that the rate of stratification has a major effect on the calculation of the loop seal clearing. Forcing the flow to be mixed

rather than stratified increases the interfacial friction between phases and more water is removed from the loop seal during the simulation. However, simply altering the limits for the flow channel inclination in which stratified flow is allowed is not a satisfactory solution to the issue. It was therefore decided that further research on the subject is needed to find an alternative method to calculate the rate of stratification.

7 RESULTS AND COMPARISON

To test the new method for calculating the rate of stratification and its effect on interfacial friction between gas and liquid phases, the simulations based on loop seal clearing experiments described in chapters 5 & 6 were repeated. In this chapter the new simulation results are presented and compared with results from experiments where possible. Results are also compared with earlier simulations.

7.1 Residual water level

The most important result from the simulations was the residual water level, which is the amount of water left in the horizontal section of the loop seal after the air/steam injection has ended. The result is so important because the residual water level can be compared directly with experimental results, and it demonstrates the practical effects of changes in rate of stratification and interfacial friction. The accurate calculation of the water level in loop seals is also important for reliable LOCA analysis.

The residual water level in IVO Loop seal experiment/simulations is shown in Figure 17.

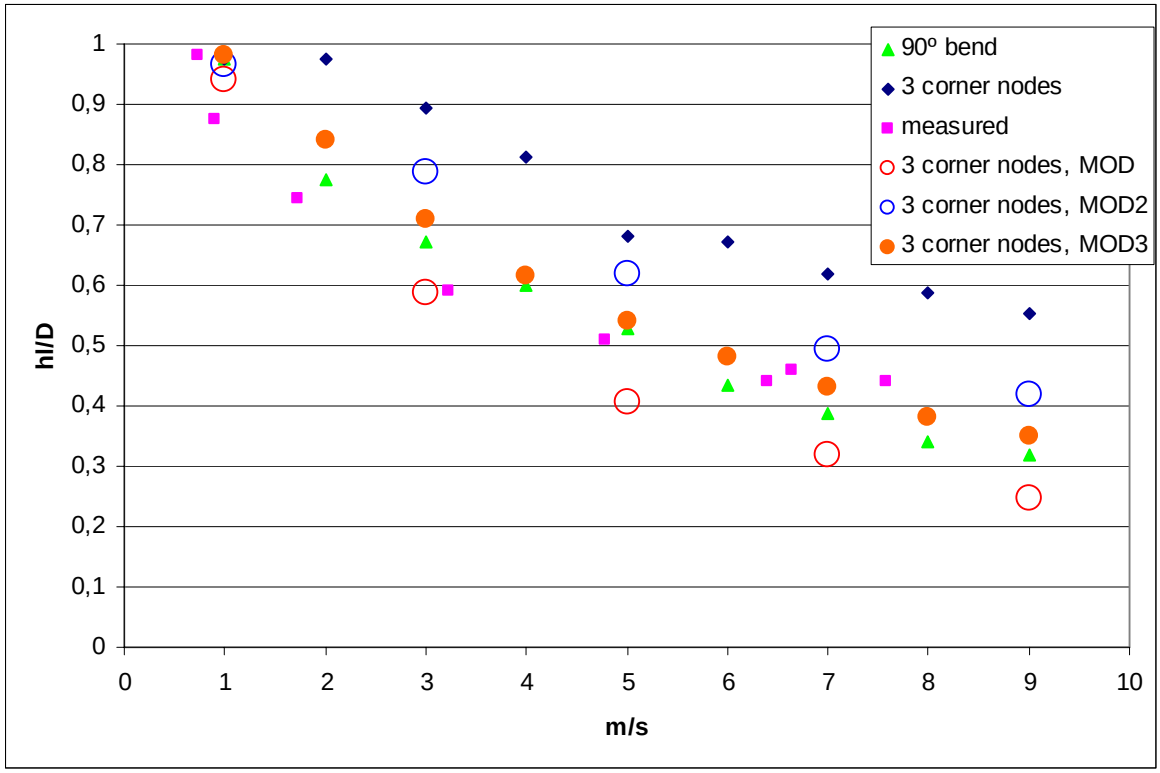

Figure 17. Residual water level in IVO Loop seal simulations and experiments.

The simulation results calculated with the new method are labelled MOD3. As can be seen, the residual water level is predicted more accurately than in earlier simulations, which either over- or underestimated the water level significantly when 3-corner node model was used. Results are particularly accurate when air flow speed exceeds 4-5 m/s. In lower velocities the simulated water level is still too high when compared to experiments, but improvement over the unmodified APROS is considerable.

The residual water level in UPTF experiment/simulations is shown in Figure 18.

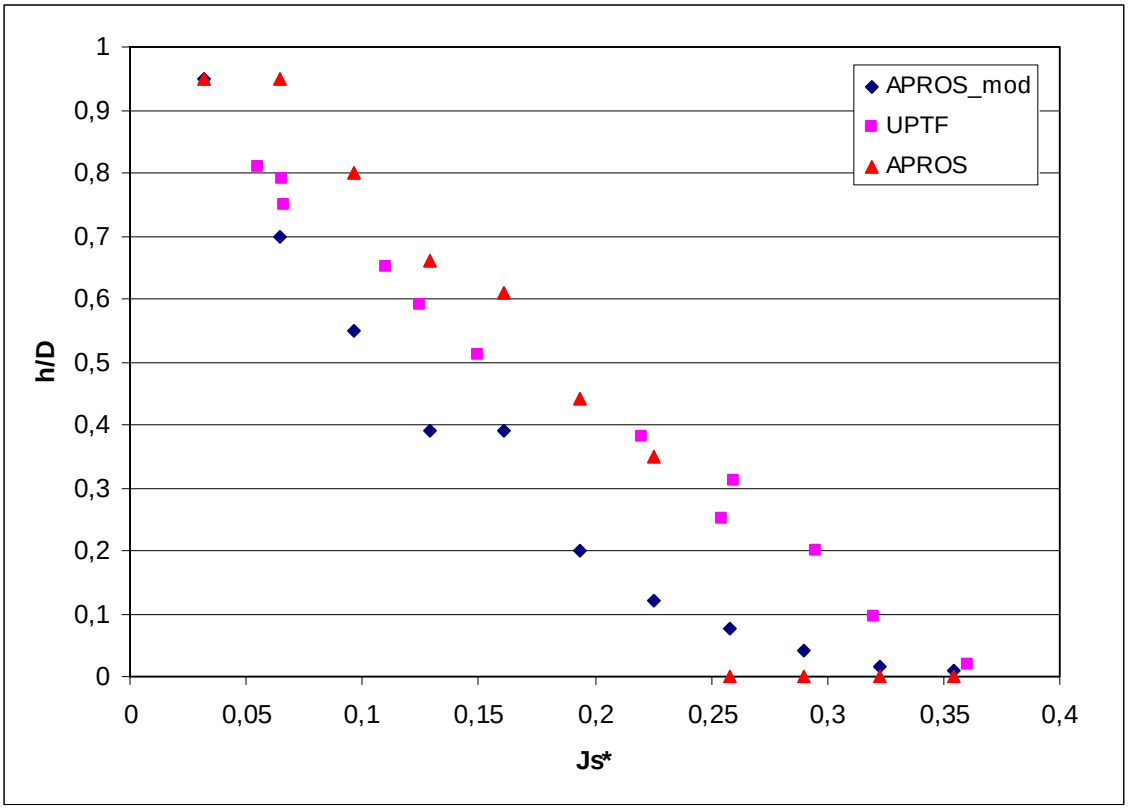

Figure 18. Residual water level in UPTF simulations and experiments.

Simulation results calculated with the new method are labelled APROS_mod. Labelling differs from the IVO case since only simulations using 3-corner node model were performed. There were two main differences between IVO and UPTF experiments and simulations. The pressure in UPTF experiments was considerably higher (15 bar) than in IVO (1 bar), and the gas injected into the loop seal was steam instead of air.

In the UPTF simulations the improvement of the results is not as significant as it was the case in IVO simulations. Nevertheless, results have improved, with the biggest change being that the loop seal is no longer completely cleared of water with mid-to-high range steam flows. APROS still underestimates the water level even with the modification, but some water does remain in the horizontal pipe. With low steam mass flows previous overestimation of the residual water level has changed into slight underestimation. Absolute difference to experimental results has decreased. With the mid-range steam flow the unmodified APROS gives better results than the modified version, as new version underestimates the water level quite drastically. Overall, the modified version of APROS

can be described as an improvement, as the complete removal of water from the loop seal when steam flows exceed the Wallis parameter of 0.25 is a significant error.

The residual water level with the modified version of APROS follows a monotonously descending curve, except for the steam velocity of 5 m/s (Wallis parameter of 0.161). Further analysis of the simulation results revealed that during steam injection the water level in the horizontal pipe is lower with a steam flow speed of 5 m/s than with a flow speed of 4 m/s (Wallis parameter of 0.129) but when the steam flow ends and residual water levels are compared, the results are identical. In other words, the faster steam flow manages to move more water from the horizontal pipe to the vertical one, but does not remove it entirely from the system. To study this deviation further, a second simulation was performed with a model which had more calculation nodes (20) in the vertical riser pipe section than in original simulations (8). The results for the residual water level in that case are shown in Figure 19.

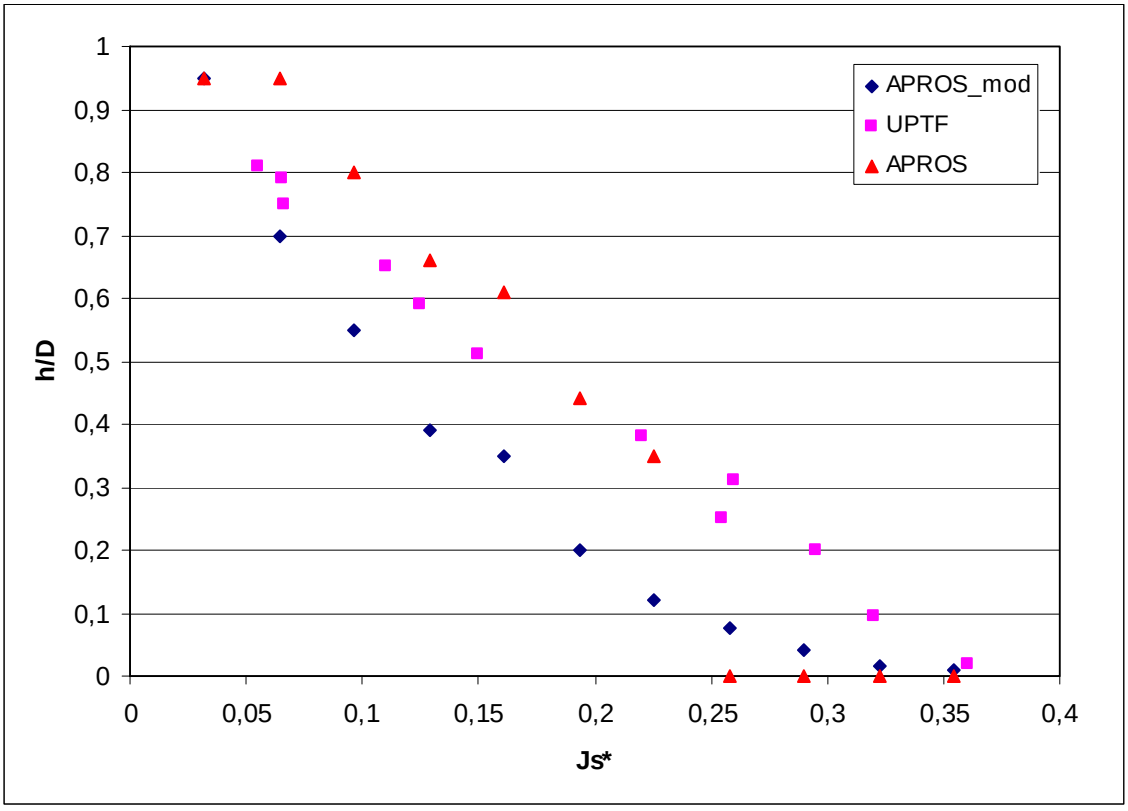

Figure 19. Residual water level in UPTF simulations and experiments with alternative nodalization.

The deviation from the general trend of the curve is now much smaller, but still noticeable.

Although the results for the change in rate of stratification are mainly displayed later (chapter 7.4), the rate of stratification in the UPTF simulations is presented here, as it is meant to illustrate the large difference between calculation methods. The rate of stratification for the second corner node (channel inclination of 45 °) is shown in Figure 20. The steam velocity in the simulation was 7 m/s, which is equivalent with a Wallis parameter of 0.23.

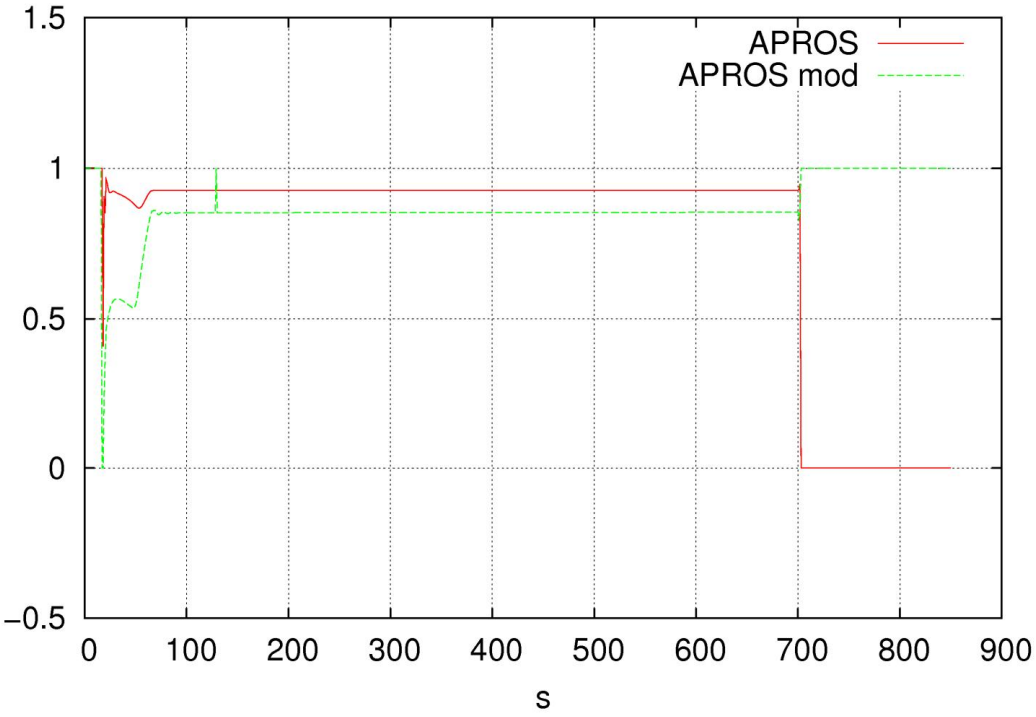

Figure 20. Rate of stratification for the second corner node in UPTF simulations.

The rate of stratification is significantly lower with the modified version of APROS. The relatively large difference in residual water level between the two APROS versions in mid-range flow speeds (Wallis parameter of ca. 0.2) can be explained with the change in the rate of stratification, but it does not explain why the current model clears the loop seal completely when flow speed increases slightly. The rate of entrainment was compared as a possible difference, but it turned out to be nearly identical between program versions (as it should, since no modification was done in that part of the source code). This kind of behaviour was not seen in the IVO simulations, which might suggest that the issue is related to steam condensation (IVO experiments used air flow instead of steam) or the higher pressure used (15 bar as opposed to the 1 bar used in IVO experiments).

7.2 Water level

The residual water level shown in the previous chapter changed significantly with the new version of APROS. It's therefore interesting to know how the water level changes during a single gas injection experiment and compare the results of the simulations. Experimental data of the water level during the loop seal clearing was not available. Water level is shown for IVO simulations using a mid-range air velocity of 5 m/s. To show the water level behaviour in different sections of the simulation model, water level is shown from four different calculation nodes: the second node for the horizontal pipe and all three corner nodes. Simulations were only made using the three corner node model.

The simulation results for the second horizontal node are shown in Figure 21.

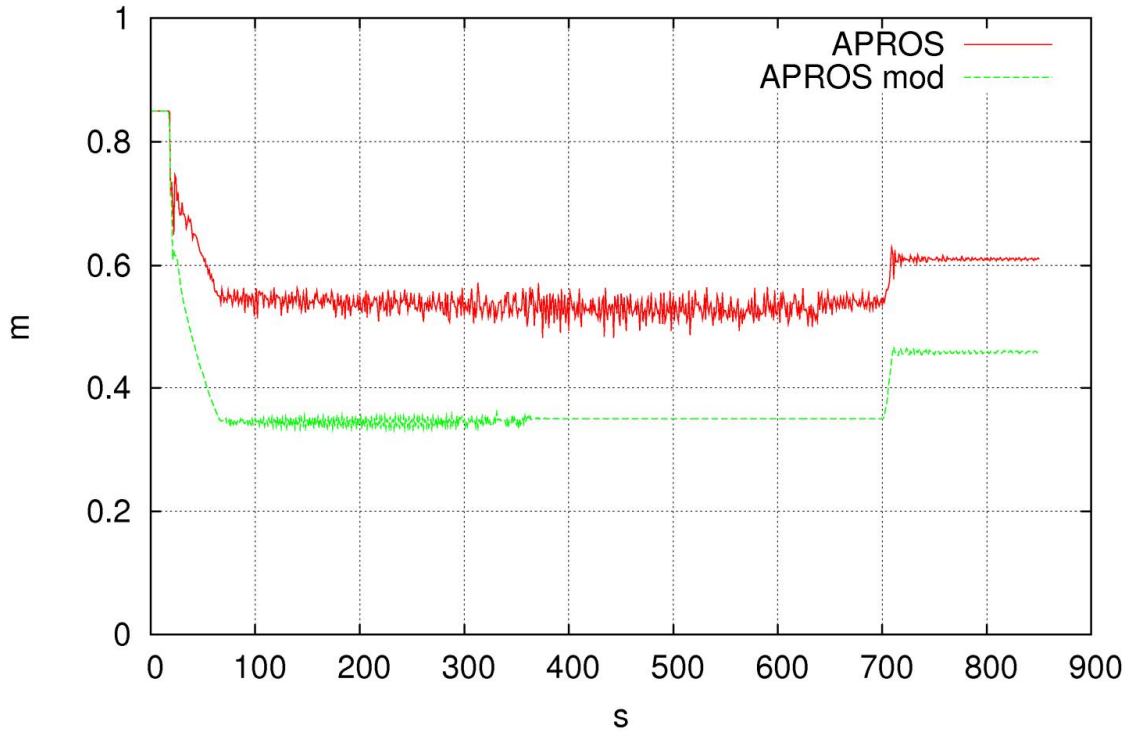

Figure 21. Water level for the second horizontal pipe node in IVO loop seal simulations.

The qualitative behaviour of water level is quite similar with the two versions of APROS. In both cases a relatively stable level is achieved in ca. 60 seconds after the beginning of the simulation. The water level is significantly lower with the modified version during the entire simulation and not just when comparing residual water levels. Difference between

the two versions is created in the simulation phase where the air flow speed is raised from 0 to 5 m/s and remains nearly constant afterwards. Oscillations are smaller with the modified version, especially in the second half of the simulation where the water level given by the modified version becomes completely stable. This is not entirely convincing, as the gas flow speed should be high enough to create some kind of wavy behaviour.

Simulation results for the first corner node (channel inclination of 27 °) are shown in Figure 22.

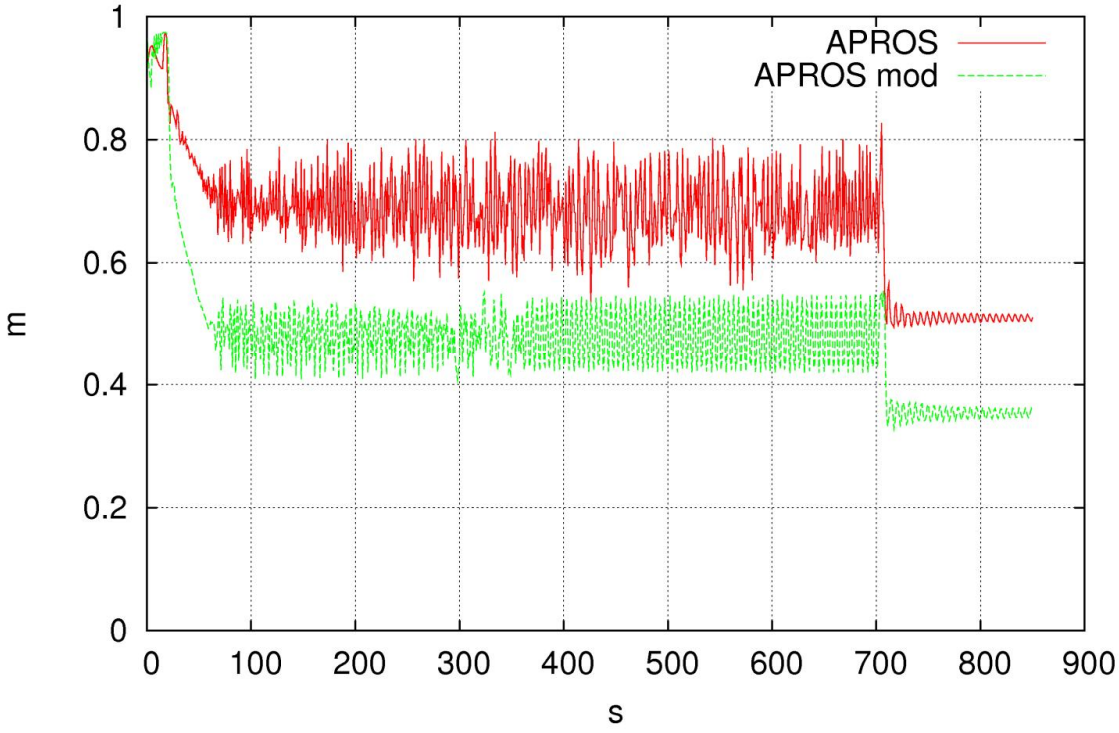

Figure 22. Water level for the first corner node in IVO loop seal simulations.

The results for the first corner node are similar to the horizontal node. Apart from the first 60 seconds, where the difference is created, the water level behaves nearly identically. Now the oscillations for the modified version are closer to the unmodified version in magnitude, and continue throughout the simulation.

The simulation results for the second corner node (channel inclination of 45 °) are shown in Figure 23.

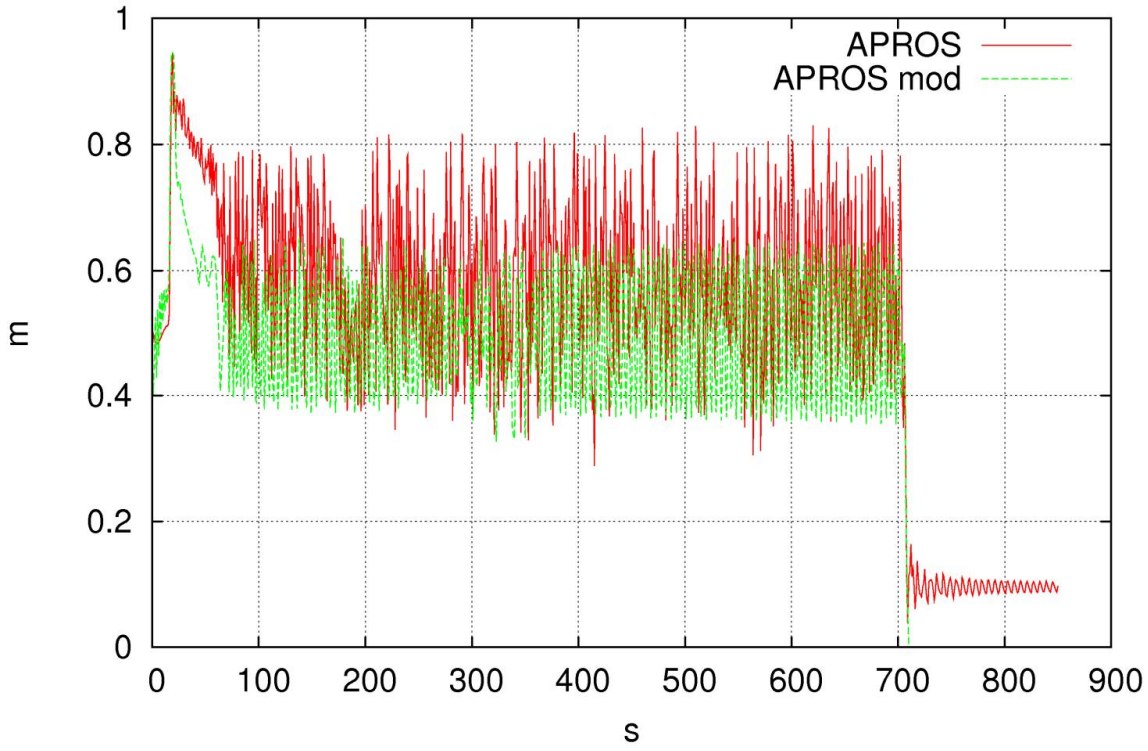

Figure 23. Water level for the second corner node in IVO loop seal simulations.

Much of the same behaviour can be seen for the second corner node. What is different is that the oscillations with unmodified version are now so large that the water levels for different versions of APROS are now overlapping. Additionally, the modified version removes all water from this node, when the unmodified version still has some left after the simulation.

The simulation results for the third and highest corner node (channel inclination of 63 °) are shown in Figure 24.

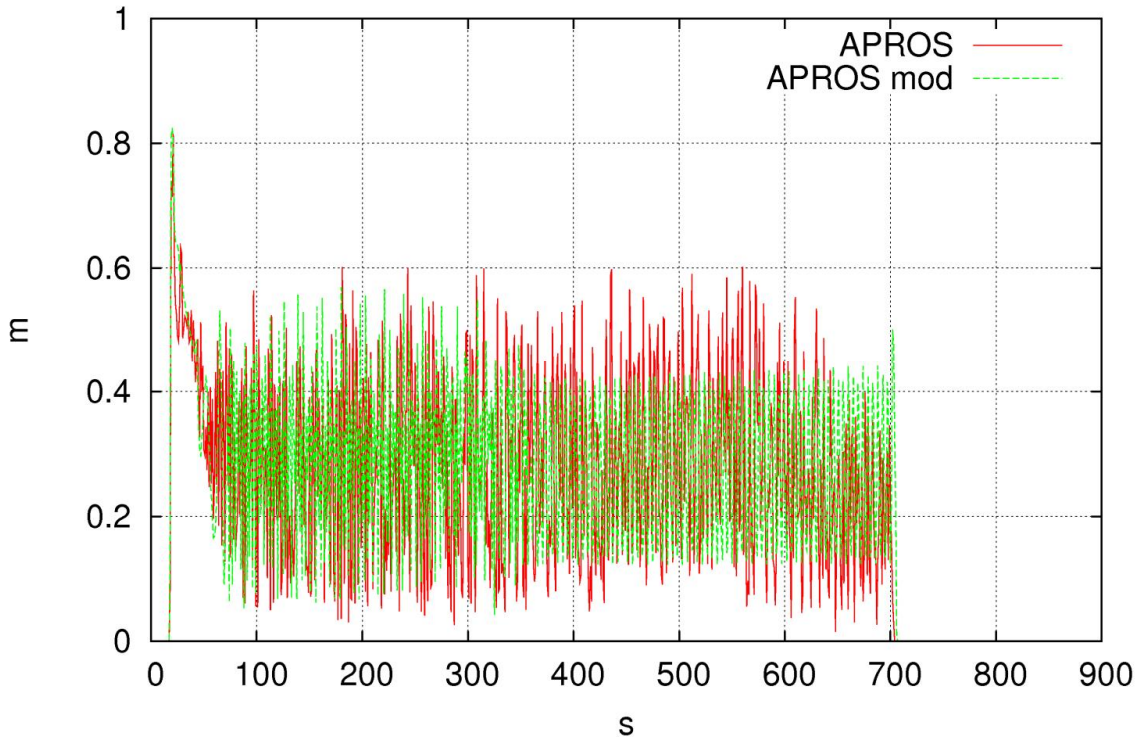

Figure 24. Water level for the third corner node in IVO loop seal simulations.

These results are the most interesting of all these water level graphs. The highest corner node is elevated so that it is empty in the beginning of the simulation, when only the horizontal section was filled with water. Therefore the water level seen in the results is due to water moving towards the riser pipe with the air flow. The results for the highest node are practically identical for the two versions; the only difference is in the magnitude of the oscillations, which is slightly smaller with the modified version, but only in the second half of the simulation. Similarity of the results is surprising considering the fact that in the other nodes the water levels were very different.

Since these results could not be compared with experimental data, they cannot be directly used to determine which of the two models is better. But considering the improvement seen in the residual water level and overall similarity of the shapes of water level graphs we can assume that the modified version does not create any unintended changes to the simulation results.

7.3 Pressure difference

Pressure difference over the loop seal can have a significant effect on core water level in LOCA scenarios, as was shown in chapter 4.2. It was shown earlier that changing the method to calculate the rate of stratification has a significant effect on the water level in the system. The water level in the loop seal affects the pressure difference, so comparing simulation results with measurements is interesting. Typical pressure difference behaviour during loop seal clearing is shown in Figure 25. The figure is from the IVO loop seal test series, and the air velocity was 5-6 m/s.

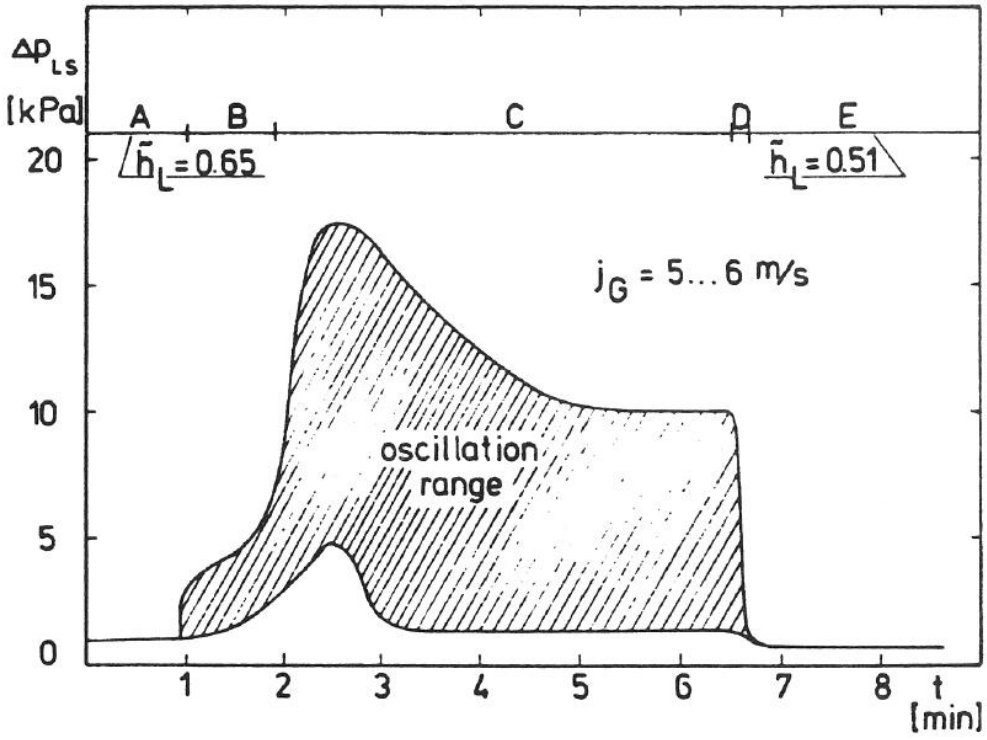

Figure 25. Pressure difference and flow regimes in IVO loop seal experiments. [Tuomisto 1988]

Regions A to E are the different flow regimes observed during the experiment. A: initial wavy stratified flow, B: transition to slug flow, C: slug flow, D: transition to stratified flow, E: stratified flow. Note that during the experiment flow is mostly in the slug flow region, i.e. it is not stratified. Results for the pressure difference for wider range of air flow speeds are shown in Figure 26.

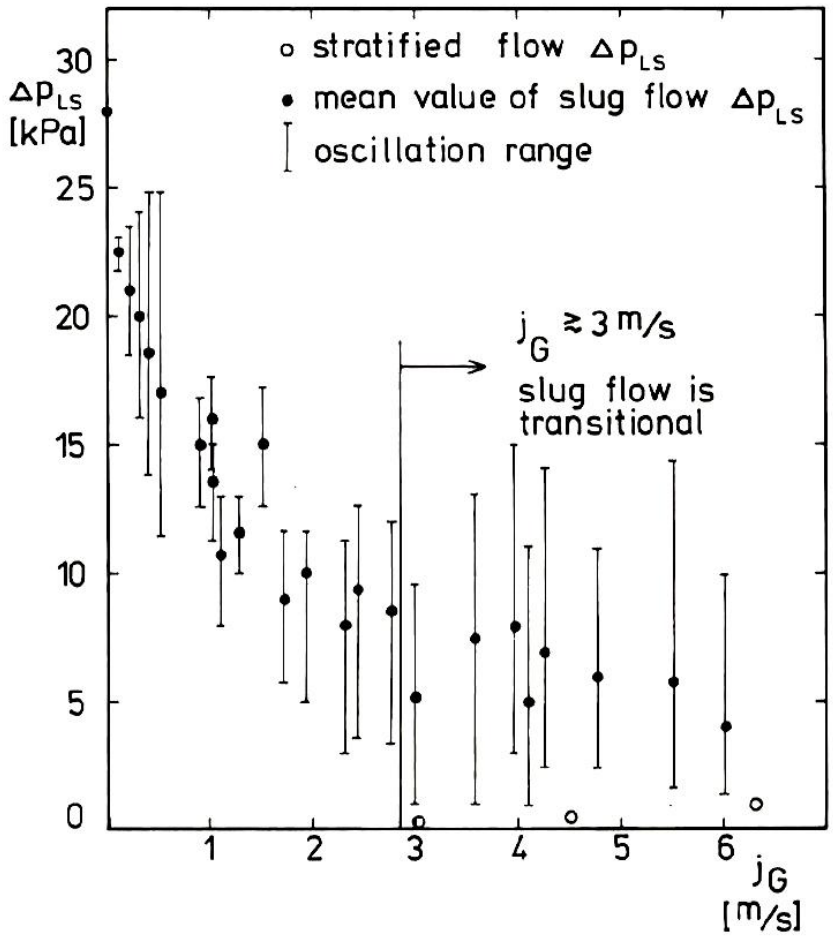

Figure 26. Pressure difference and oscillation range in IVO loop seal experiments. [Tuomisto 1988]

As it can be seen, the mean value for pressure difference decreases and pressure oscillation increases as the gas flow speed increases. The pressure difference does not have a stable value during the experiment. This is due to the nature of the slug flow in the horizontal pipe section, shown in Figure 27.

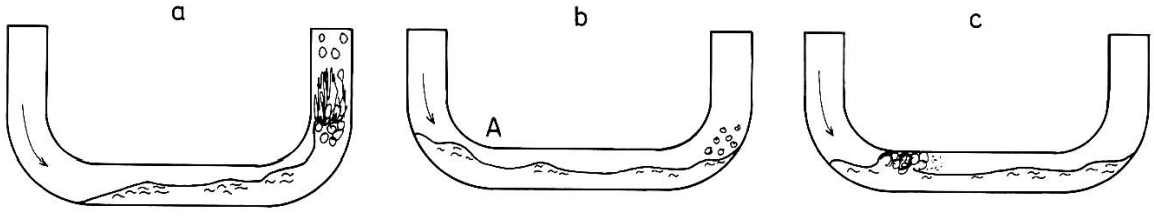

Figure 27. Slug flow oscillation during loop seal clearing. [Tuomisto 1988]

In stage a) gas flow has pushed the water into the vertical riser pipe, but if the gas flow is not strong enough, water will flow back to the horizontal section instead of exiting the loop seal. In stage b) a new slug is formed in area A, when water level oscillation causes the pipe cross section to be completely filled with water. In stage c) the new slug is beginning to move as the gas flow pushes it towards the riser pipe. Pressure difference over the loop seal is considerably different between these three stages. [Tuomisto 1988]

The simulation results for the pressure difference in IVO loop seal with the unmodified APROS are shown in Figure 28. To keep the graph readable the amount of flow speeds shown is limited to three.

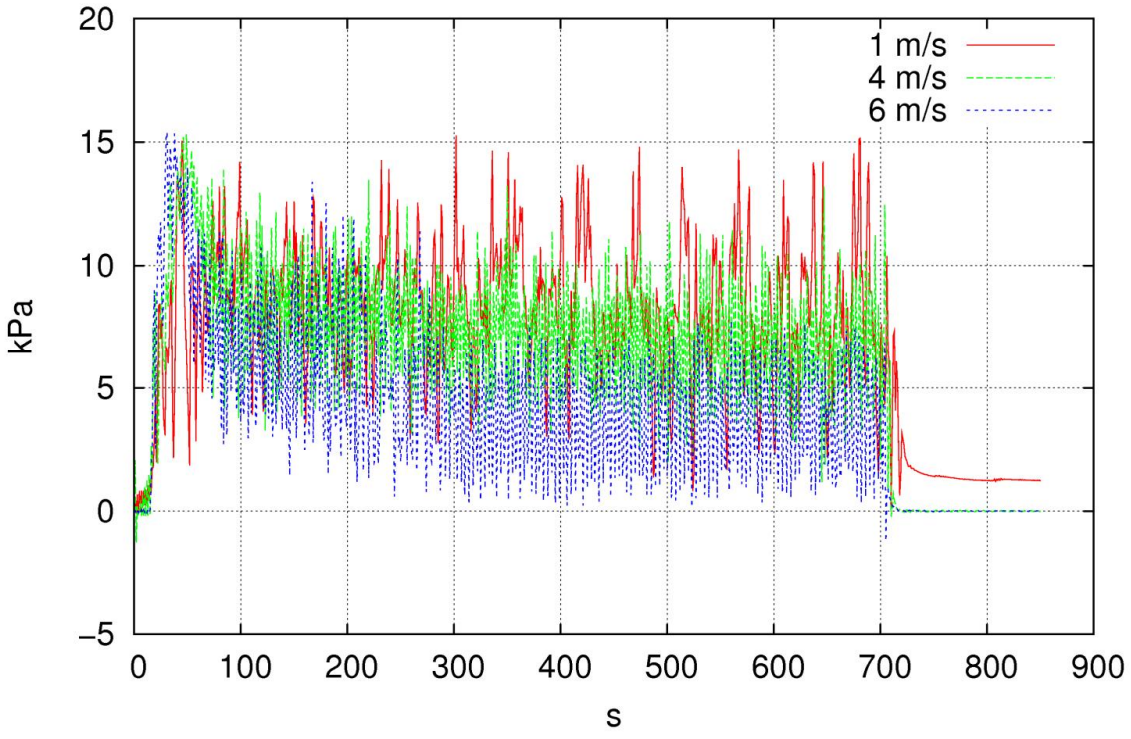

Figure 28. Pressure difference in IVO loop seal simulations with unmodified APROS.

The simulated pressure difference matches quite well with the experimental results. The mean value for the pressure difference in low and high flow speeds is underestimated slightly, but in mid-range the simulation results seem accurate. Oscillation range does not seem to follow the trend set by the experiments, as the range does not increase with flow speed but rather decreases. The magnitude of the oscillations is relatively accurate.

Simulation results with the modified APROS are shown in Figure 29.

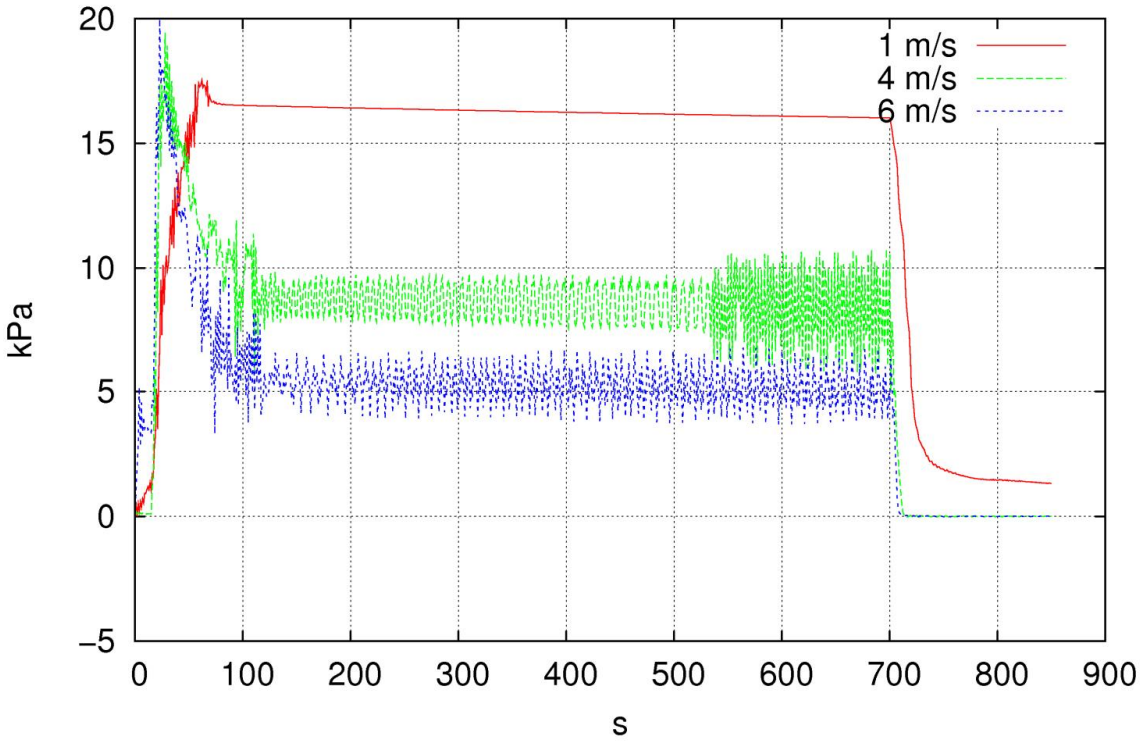

Figure 29. Pressure difference in IVO loop seal simulations with modified APROS.

Mean value for the pressure difference is now relatively accurate across the flow speed range. However, the amplitudes of pressure oscillation are not large enough in any of the cases, especially in the 1 m/s case in which pressure does not oscillate at all. This is most likely due to the fact that as more water is being removed from the loop seal with the modified version (lower water level) the slug flow oscillations shown in Figure 27 are not as significant.

To judge which of the two versions is better in the pressure difference calculation is not simple. Both have difficulties in different areas of pressure difference calculation. The unmodified version is better at predicting pressure oscillations and the modified version calculates the mean pressure difference more accurately. It is difficult to estimate which characteristic is more important in safety related simulations. In LOCA simulations the mean pressure difference is most likely more important than the amplitude and frequency of the pressure oscillation, since the relatively large water mass and flow cross-sections in the pressure vessel prevent rapid oscillations in the core water level. The core water level is

affected more by the mean pressure difference over the loop seal than the pressure oscillations.

Similar measurements were also performed on the UPTF experiments. The pressure drop across the loop seal after initial clearing is shown in Figure 30 as a function of the Wallis parameter.

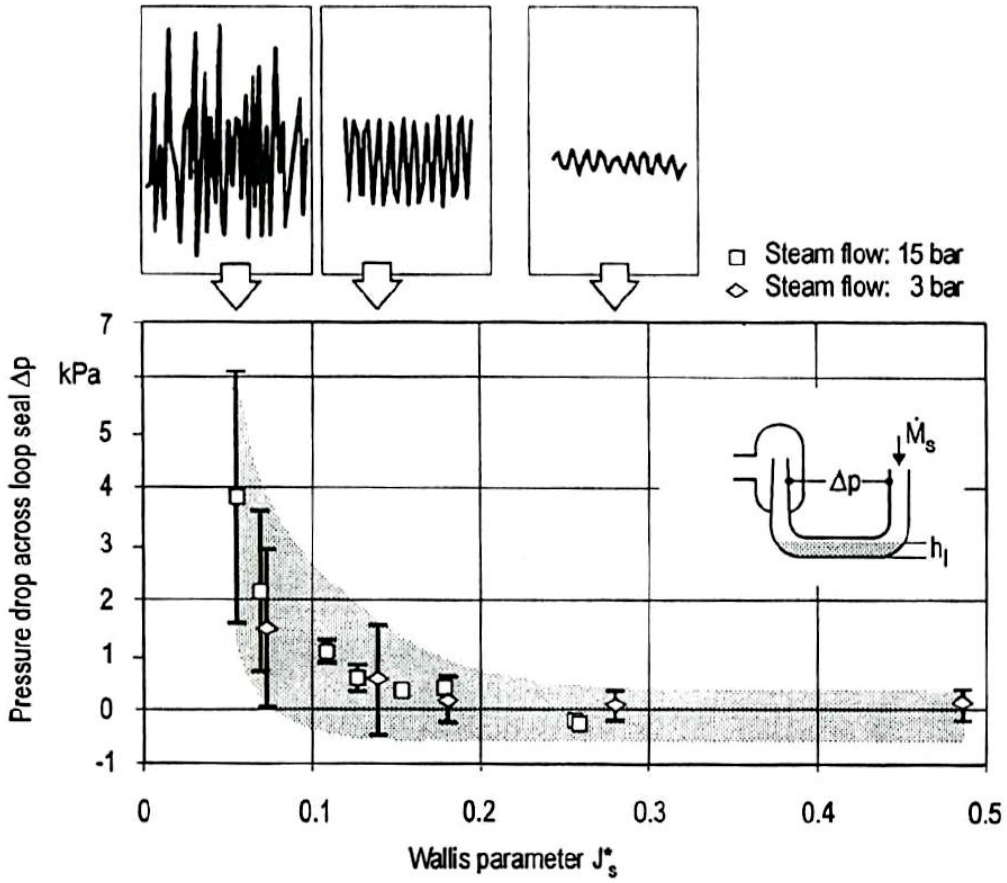

Figure 30. Pressure difference in UPTF experiments. [Liebert 1998]

As opposed to the IVO experiments, the measured pressure oscillation range decreases as the steam mass flow increases. Otherwise the behaviour is similar, mean pressure difference decreases as gas flow through the loop seal increases.

The simulation results for the unmodified APROS are shown in Figure 31. Simulation results are shown for steam velocities 2, 5 and 8 m/s. The corresponding values for Wallis parameter are 0.065, 0.161 and 0.258. Also, simulations were only run on 15 bar pressure, so comparison should only be made with those experimental results.

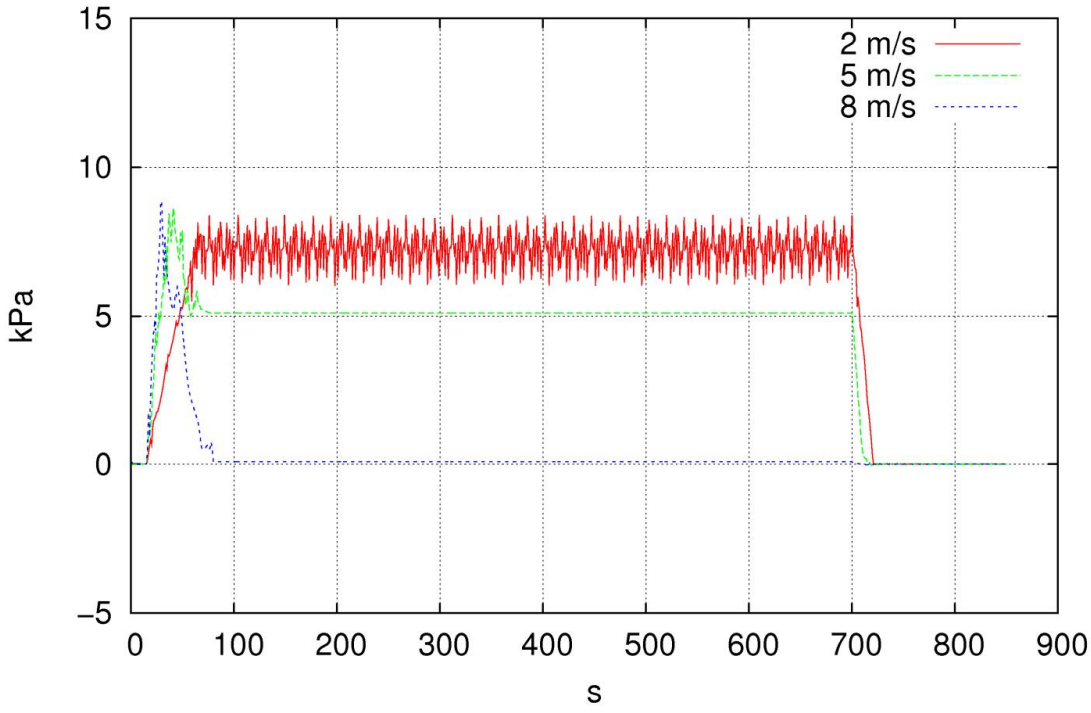

Figure 31. Pressure difference in UPTF simulations with unmodified APROS.

The unmodified APROS seems to overestimate the pressure loss for low and medium steam flows. This is to be expected, since the unmodified APROS does not remove enough water from the system during steam injection. More water in the pipes leads to larger pressure loss across the loop seal. For 2 m/s the difference is the largest: a mean pressure loss of 4 kPa was measured (with significant oscillation), when APROS gives a value of ca. 7 kPa with slightly smaller oscillation. The difference decreases as steam velocity increases, and for 8 m/s the results are nearly identical at 0 kPa. It is noteworthy that the pressure oscillations seem to disappear completely in the experiments with 15 bar pressure when Wallis parameter exceeds the value of 0.15. This is the complete opposite of the oscillation behaviour seen in IVO experiments where oscillation magnitude increased as air velocity increased. Simulation results are in good agreement with the experiments, as they show no pressure oscillation at all with high steam flow speeds.

The simulation results with modified APROS are shown in Figure 32.

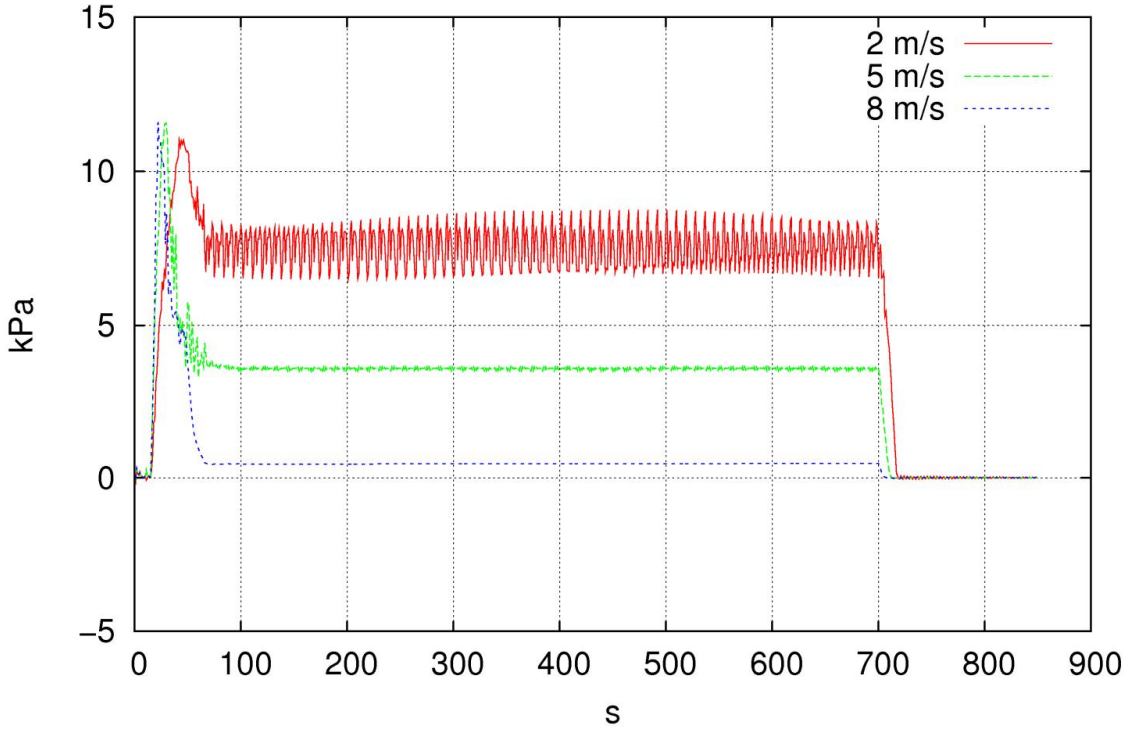

Figure 32. Pressure difference in UPTF simulations with modified APROS.

There does not seem to be much difference in simulation results between the two APROS versions. The pressure difference is lower with medium steam flow and closer to the experimental results, but slightly higher with high steam flow. Biggest difference is in the behaviour of pressure difference in the beginning of the simulation. Modified version gives a higher peak value for all velocities shown before settling down.

As it was the case in IVO simulations, clear improvement to simulation results when using the modified version of APROS was not achieved. The comparison with experiments shows that neither model gives very good results for low and medium steam flows, and the results for high steam flow are nearly identical.

7.4 Rate of stratification

As the method for calculating the rate of stratification was altered, it is obviously necessary to compare how the actual values behave. This simulation result can not be directly compared with experimental result, as this is not a measurable quantity, or at least it was not measured in the IVO nor UPTF test series. Rate of stratification is shown for IVO simulations using a mid-range air velocity of 5 m/s and four different calculation nodes: the second node for the horizontal pipe and all three corner nodes.

The simulation results for the second horizontal node are shown in Figure 33.

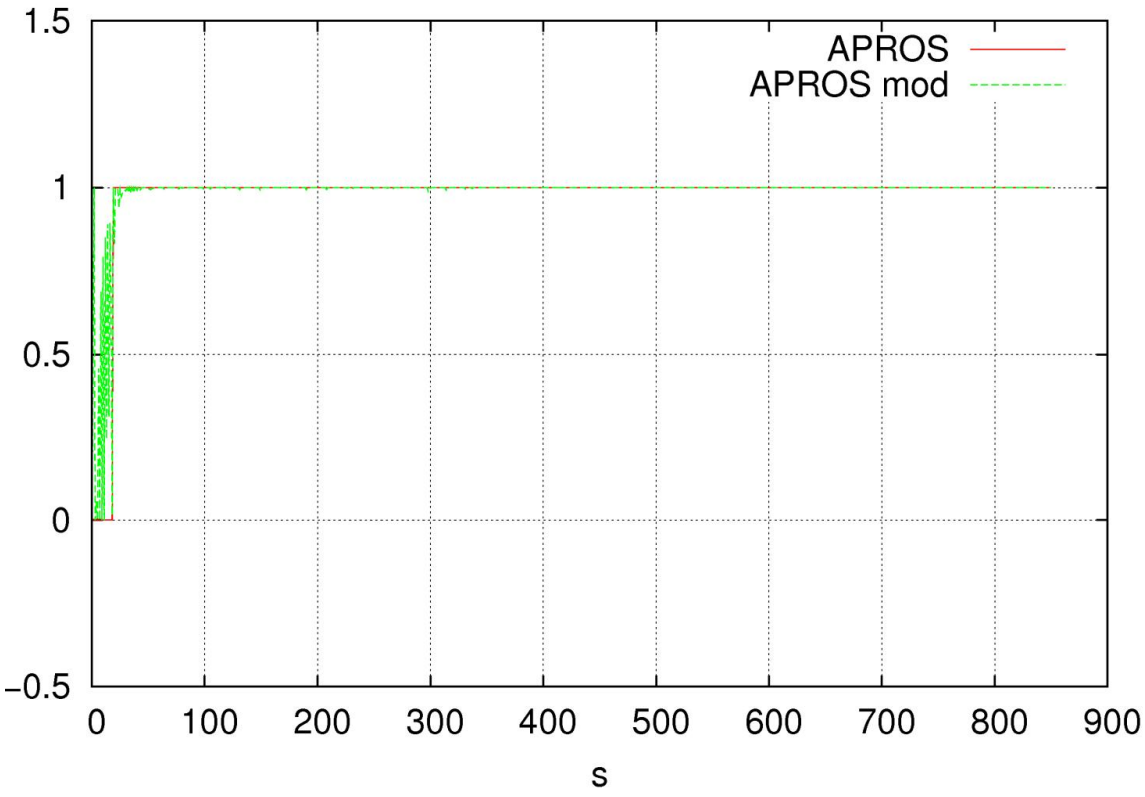

Figure 33. Rate of stratification for the second horizontal pipe node in IVO loop seal simulations.

The only difference between APROS versions is in the first 50 seconds of the simulation, when unmodified APROS displays an abrupt jump from 0 to 1. The modified version moves from 0 to 1 through several oscillations. From there on, both models give identical results; the flow is calculated as stratified in the horizontal pipe. If we compare this with

the visual description of the flow regime (Figure 25), both models give a wrong result as the majority of the test for 5-6 m/s was described as slug flow.

The simulation results for the first corner node (channel inclination of 27 °) are shown in Figure 34.

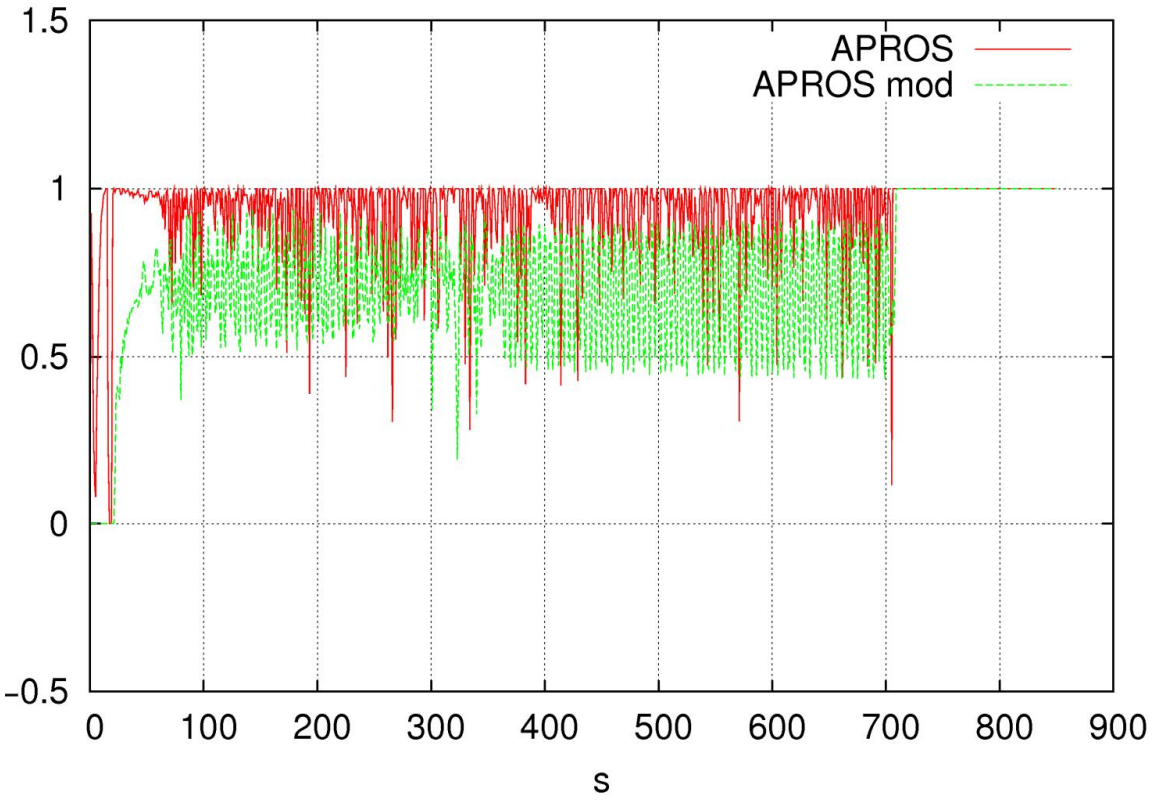

Figure 34. Rate of stratification for the first corner node in IVO loop seal simulations.

Now the results are significantly different. The unmodified APROS gives a higher value for the rate of stratification throughout the experiment than the modified version. This means that the modified version calculates the flow in the corner node as somewhat mixed, while the unmodified version remains almost entirely as stratified flow. This should have a noticeable effect on the calculation of interfacial friction.

The simulation results for the second corner node (channel inclination of 45 °) are shown in Figure 35.

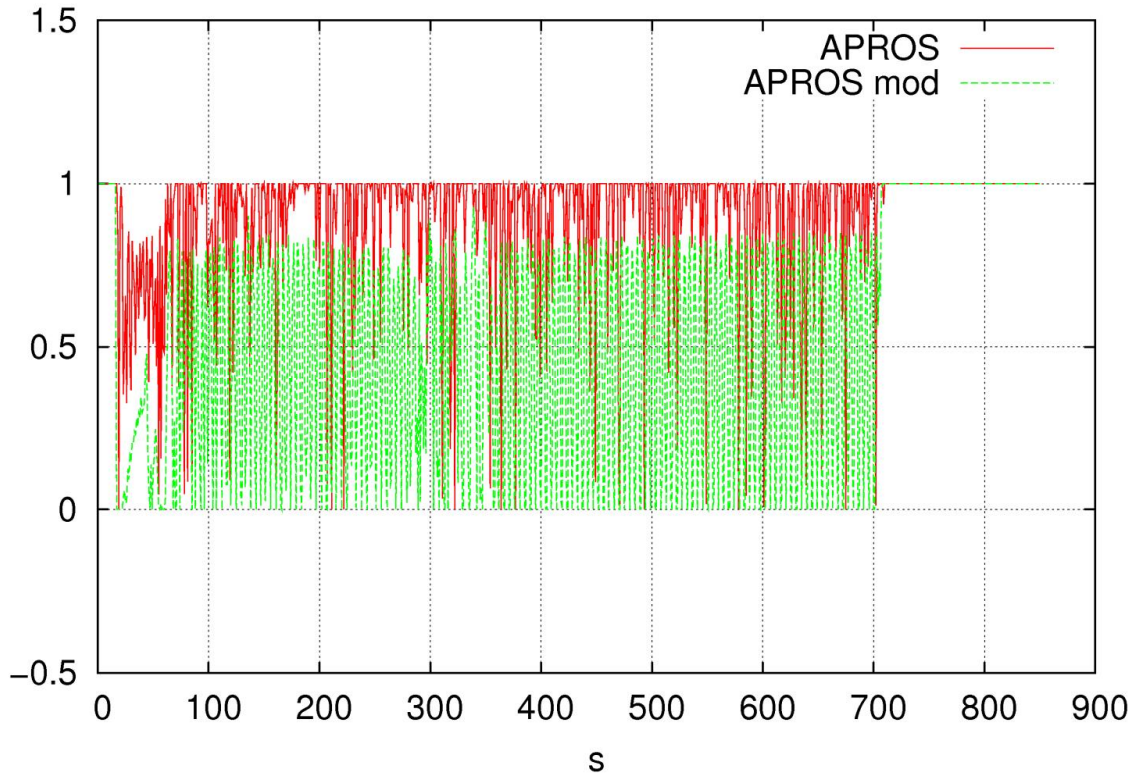

Figure 35. Rate of stratification for the second corner node in IVO loop seal simulations.

The results for the second corner node are similar to those of the first corner node. Again the unmodified version calculates higher values for the rate of stratification than the modified version. Now the values for the modified version are even smaller, which means the flow regime is even more towards intermittent flow. The unmodified version gives some low values as well, but the vast majority are still very close to fully stratified flow.

The simulation results for the third and highest corner node (channel inclination of 63 °) are shown in Figure 36.

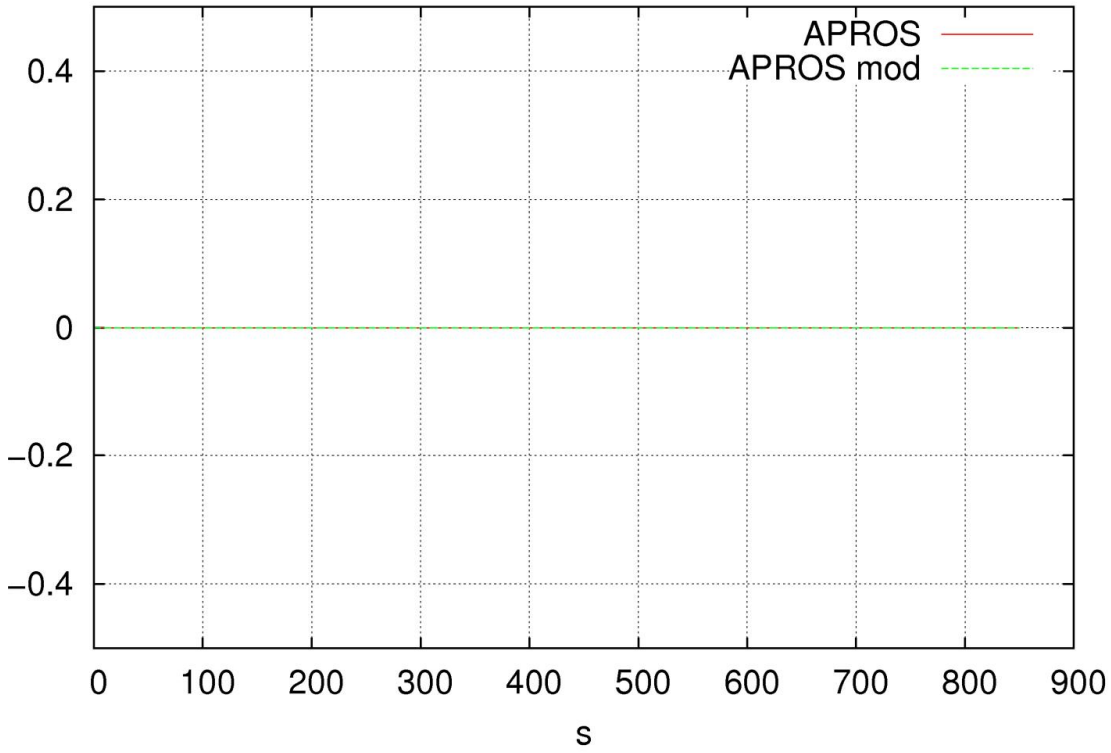

Figure 36. Rate of stratification for the third corner node in IVO loop seal simulations.

With this corner node both models give identical results, giving 0 for the entire simulation run. This is because both models have a maximum value for the channel inclination for which stratified flow is allowed, and that limit is ca. 60 degrees. The inclination in this node exceeds that limit, so rate of stratification is forced to 0.

7.5 Interfacial friction

As shown earlier in chapter 2.4, rate of stratification is used as a weighting coefficient when calculating the interfacial friction coefficients in the system. As the values for rate of stratification are so different with the modified version of APROS, it's interesting to see how this affects the interfacial friction in the flow channel. The interfacial friction strongly affects the amount of water which clears the loop seal in the simulation, and is therefore shown here. No experimental results were available for this quantity, so comparison between calculation methods is the only result shown.

As opposed to earlier results, interfacial friction is not calculated in the nodes, but in branches of the simulation model. Therefore the comparison is shown in a horizontal branch, and all four corner branches. The simulation model used is again the IVO facility, using a mid-range 5 m/s air velocity.

The interfacial friction in a horizontal branch is shown in Figure 37.

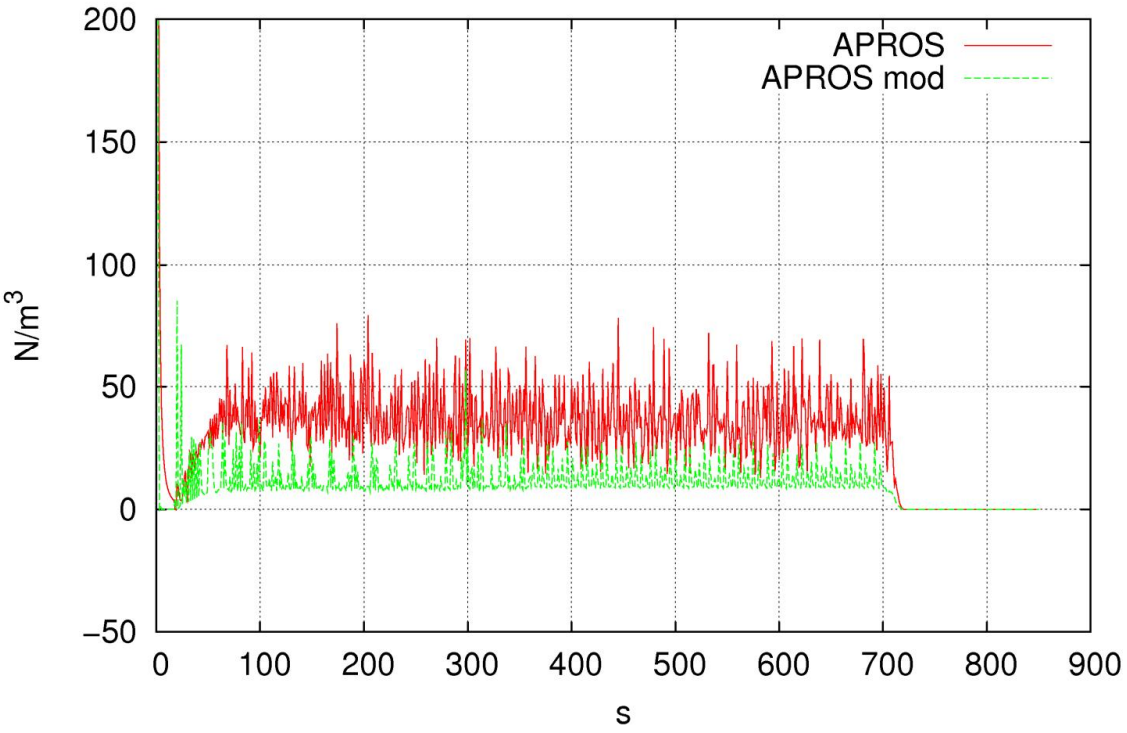

Figure 37. Interfacial friction in a horizontal branch in IVO loop seal simulations.

Both models start with a large spike in the interfacial friction. This is due to the initial injection of air into the water-filled channel. After initial clearing, when flow conditions have stabilized, unmodified APROS gives noticeably higher values than the modified, but as we see later, values given by both models are rather small. This indicates stable flow conditions without much turbulence or other mixing phenomena.

The interfacial friction in the first corner branch (inclination of 18 °) is shown in Figure 38.

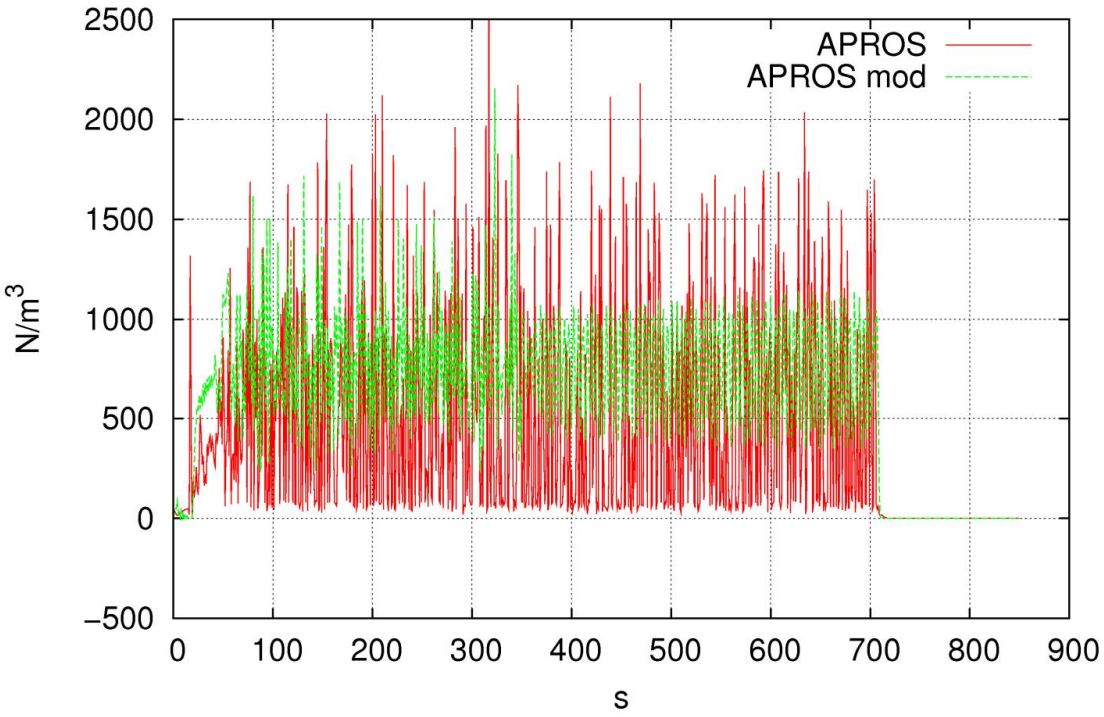

Figure 38. Interfacial friction in the first corner branch in IVO loop seal simulations.

The magnitude of the interfacial friction jumps immediately when the flow channel is inclined. Both models present spikes which exceed 2000 N/m^3. What's different between the two APROS versions is that the modified version gives higher minimum values; ca. 400 N/m^3, when the unmodified version gives minimum values of ca. 50 N/m^3. This difference seems to be responsible for the lower water levels achieved with the modified version. The oscillation range of the interfacial friction calculated with unmodified version is significantly greater than with the modified version.

The interfacial friction in the second corner branch (inclination of 36 °) is shown in Figure 39.

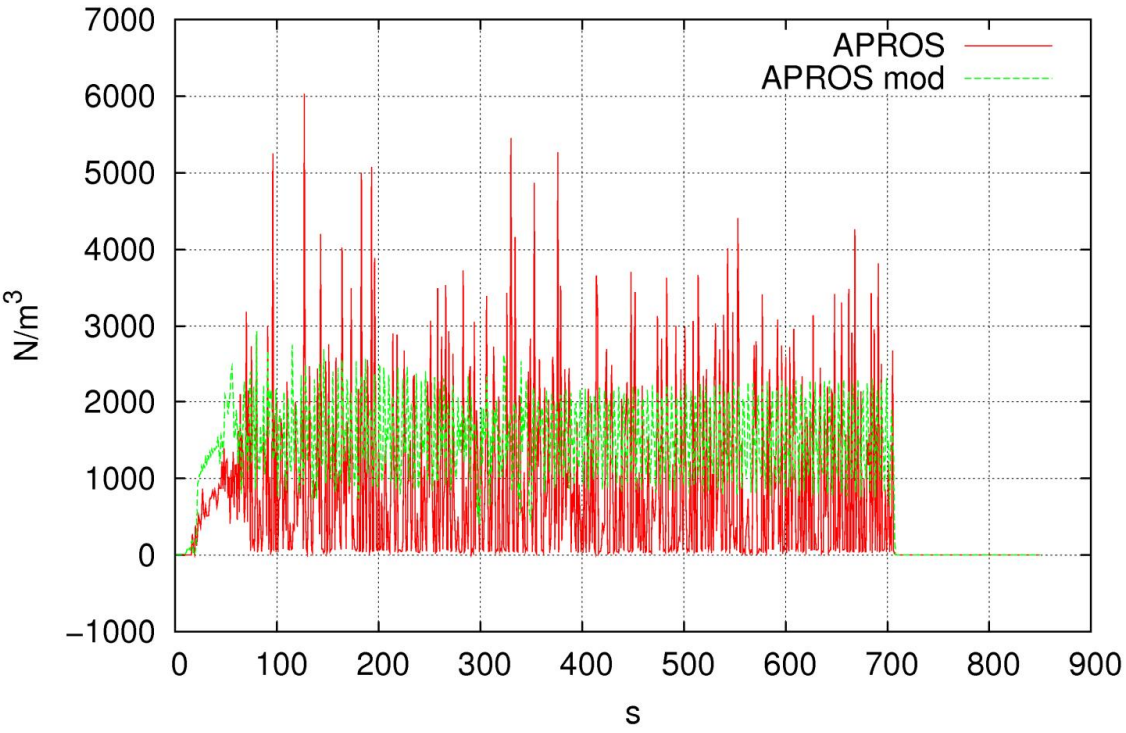

Figure 39. Interfacial friction in the second corner branch in IVO loop seal simulations.

The results here are quite similar to those in the previous corner node. The values of the spikes are now even higher, especially those of the unmodified version. More importantly, the difference in the minimum values is now roughly 1000 N/m^3, as the modified version gives the larger values. Values given by the modified version are also significantly higher in the first 100 seconds of the simulation, and as a consequence more water has been removed from the system, which can be seen in Figure 23.

The interfacial friction in the third corner branch (inclination of 54 °) is shown in Figure 40.

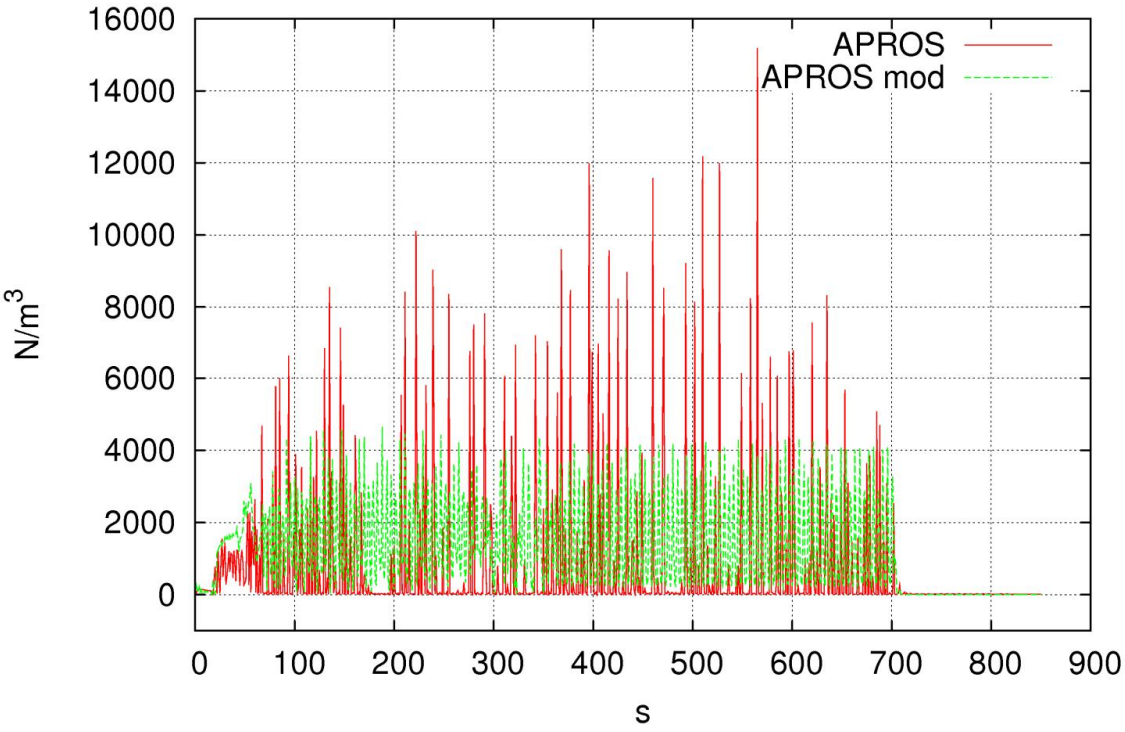

Figure 40. Interfacial friction in the third corner branch in IVO loop seal simulations.

The results for the third branch offer no surprises, either. Spike values keep growing, especially for the unmodified version, but the modified version gives the higher overall values.

The interfacial friction in the fourth and highest corner branch (inclination of 72 °) is shown in Figure 41.

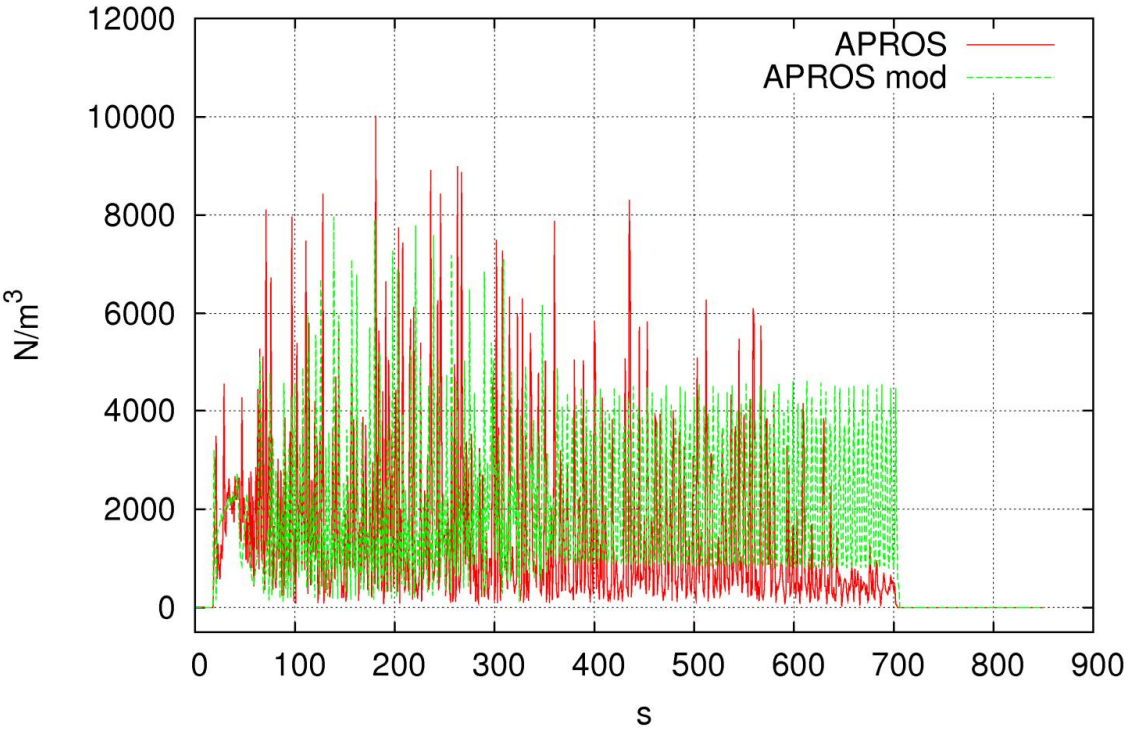

Figure 41. Interfacial friction in the fourth corner branch in IVO loop seal simulations.

Interestingly the results for the final branch are very similar. But as was shown in Figure 36, when the channel inclination exceeds 60 degrees, the rate of stratification is forced to 0 in both models. This is now the case, and as the change in rate of stratification was the only difference between the APROS versions, similarity of the results is no surprise. The difference in the values for the second half of the simulation, where modified version gives higher minimum values could be related to the lower water inventory in the system.

Again, as these simulation results could not be compared against experimental results, they can not be directly used to decide the superiority of the calculation methods. They were shown only to illustrate how changing the rate of stratification affects the simulation.

8 VALIDATION

Validation of APROS is based on simulating a wide range of well known test cases, of which some are separate effect test scenarios and some entire power plants. Since the code change made during this project is not very large, a complete set of validation tests was not calculated. Instead, two separate effect test cases were simulated with the unmodified and modified version to see if the modification has any unwanted effects on the simulations. When the change made here is implemented into official version of APROS, it will go through the complete validation procedure with all the other code changes made since the release of a previous version.

In this chapter, two of the separate effect test cases and simulation results are briefly introduced.

8.1 Battelle top blowdown experiment

First of the two separate effect test cases is the Battelle top blowdown experiment (OECD Standard Problem No.6). Purpose of the experiment is to demonstrate the rise of water level in a BWR in the case of sudden depressurization. Schematic with dimensions of the Battelle test vessel is shown in Figure 42.

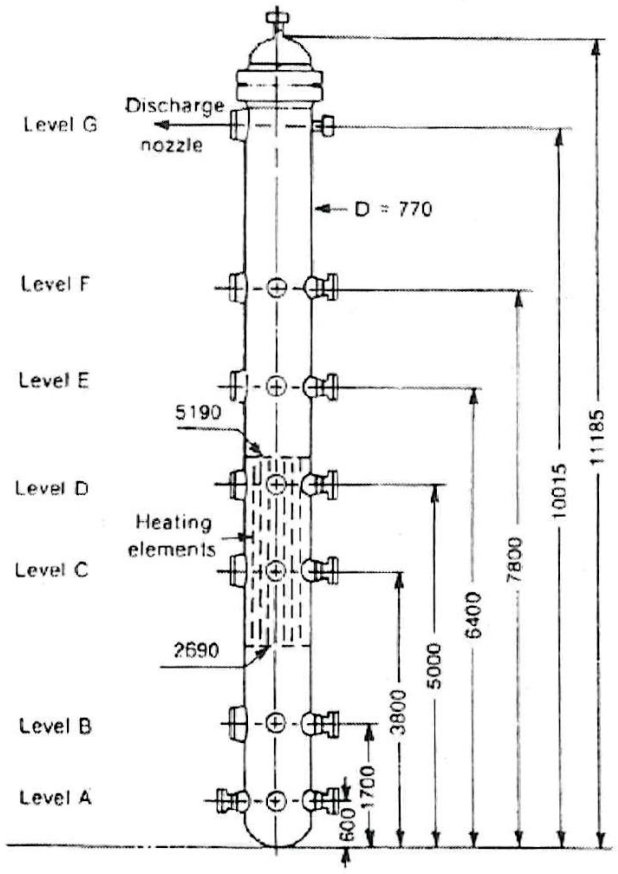

Figure 42. Test facility of the Battelle top blowdown experiment. [Siikonen, Kantee 1983]

The test vessel has an inner diameter of 0.77 m and a height of 11.19 m. In initial conditions the vessel is in a pressure of 7.07 MPa and at a temperature of 285 °C. Initial water level is 7.07 m. Test begins when the break orifice in the discharge nozzle (level G, height of 10.01 m) is opened. As the pressure in the vessel decreases, the water level starts to rise. When the water level reaches the height of the nozzle, a sharp increase is seen in the break mass flow. Accurate simulation of the break mass flow is the main point of interest in this validation case. [Hölzer 1977]

The simulations based on the Battelle top blowdown experiment were calculated with the unmodified and modified versions of APROS. As expected, the results are identical, as changing the method for calculating the rate of stratification should not affect this test case. This test was used just to see if any unintentional changes were made. As there was absolutely no difference in the simulation results between versions which would require

further commentary, the results are not shown here, but instead in Appendix I. Results simulated with the modified version of APROS are labelled “6 eq mod”.

8.2 Edwards pipe

Edwards pipe is a horizontal pipe, which is initially closed at both ends. Schematic with dimensions of the Edwards pipe test vessel is shown in Figure 43.

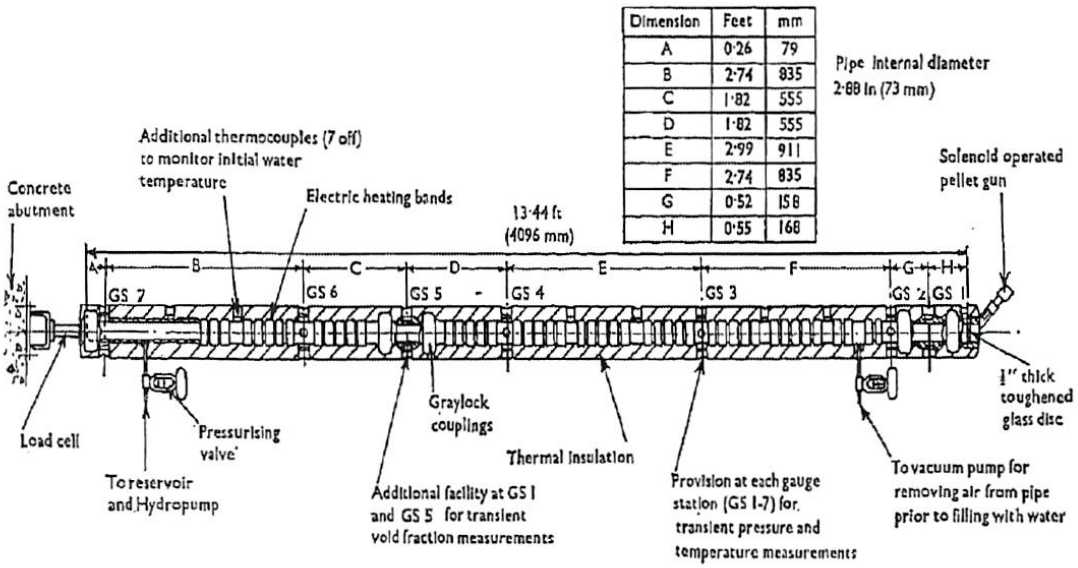

Figure 43. Edwards pipe test facility. [Edwards, O'Brien 1970]

Test vessel has a length of 4.096 m and a diameter of 0.073 m. In initial conditions the pipe is filled with water. The pressure is 6.895 MPa and the temperature 242 °C. The test begins when the pellet gun mounted on the one end of the pipe (seen on the right in Figure 43) shatters the glass disc which closes the pipe. The rapid depressurization causes the water to evaporate and flow out of the tube with high velocity. Main point of interest in these simulations is the accurate calculation of pressure in both ends of the pipe during the discharge. [Edwards, O'Brien 1970]

The simulations based on the Edwards pipe experiment were calculated with the unmodified and modified versions of APROS. As was the case with Battelle simulations, no difference between versions was seen here either. This is good, since the unmodified

version manages to calculate the test case well. The results are shown in Appendix II. Results simulated with the modified version of APROS are labelled “6 eq mod”.

9 CONCLUSIONS

Modelling two-dimensional phenomena (such as phase stratification in a flow channel) with a one-dimensional system code (such as APROS) has always some inaccuracies and room for improvement. This thesis focused on improving the calculation of rate of stratification in APROS. A brief description of the six-equation model and the calculation methods for two-phase flow were also presented. Inaccuracies of the current APROS were discovered in loop seal simulations, so it was also necessary to briefly describe the phenomena and behaviour related to them, especially in the context of nuclear power plants. Introducing the new method for the calculation of rate of stratification and the simulation results achieved formed the core of the thesis.

The residual water level in loop seal simulations was one of the few parameters where experimental results were available for comparison. It is also vital when water inventory in the primary circuit is considered. It was therefore the natural choice as the main result used to define the accuracy of the calculation method. In this aspect, the new method implemented during this thesis project is more accurate than the one used in current APROS. The simulation results for the IVO loop seal experiments showed the most improvement, as the simulation no longer overestimates the water level as significantly than the previous version. Results for the UPTF can also be described as an improvement, since the complete clearing of the loop seal which did not occur in the experiments was now avoided in the simulations as well.

Pressure difference was the only other parameter which was available for comparing the simulation results with experiments. In this aspect the comparison between the methods for calculating the rate of stratification is difficult, since neither model gives accurate results. The method applied in the current APROS predicts the pressure oscillations fairly well, but the new method is more accurate when calculating the mean pressure difference.

The rate of stratification calculated by the new method tends to give smaller values in the simulations performed than the previous method, i.e. the phases are more mixed with the new version. This leads to higher mean values of interfacial friction, which in turn leads to smaller residual water levels as more liquid is ejected from the loop seal during the

simulation. Since the overestimation of the water level was the biggest initial problem, the new method can be described as an improvement.

The lack of experimental results was probably the most challenging aspect of this thesis. While the residual water level is a good variable for comparing the simulations with experiments after the gas injection has ended, it can not be used to estimate the behaviour of the system during gas injection, while water is still being removed from the system. Deciding whether the new model is an improvement or not based on such a small amount of experimental data is not easy, especially when the few comparable parameters give mixed results. Before the new method can be accepted into official version of APROS, additional validation is needed.

REFERENCES

Anoda, Y., Kukita, Y., Nakamura, N. & Tasaka, K. 1989. Flow regime transition in high-pressure large diameter horizontal two-phase flow. ANS Proc. Philadelphia, Pennsylvania, 6-9 Aug. National Heat Transfer Conference. ISBN 0-89448-149-5.

Bestion, D. 1990a. Description Generale Des Lois Physiques Du Module De Base. ISSN SETh/LEML-EM/89-190.

Bestion, D. 1990b. The physical closure laws in the CATHARE code. Nuclear Engineering and Design, Vol. 124, No. 3, pp. 229-245. ISSN 00295493.

Edwards, A.R. & O'Brien, T.P. 1970. Studies of phenomena connected with the depressurization of water reactors. Journal of British Nuclear Society, Vol. 9, No. 2, pp. 125-135.

Haapalehto, T. 1995. Validation studies of thermal-hydraulic code for safety analysis of nuclear power plants. Lappeenranta: Lappeenrannan teknillinen korkeakoulu. ISBN 951-763-980-5 (nid.).

Hewitt, G.F. & Hall-Taylor, N.S. 1970. Annular two-phase flow. Oxford: .

Hillberg, S. 2009. Full Scale Loop Seal experiments with TRACE V5p1 and APROS 5.08. Espoo: VTT Technical Research Centre of Finland.

Hillberg, S. & Hänninen, M. 2010. Virtauksen erottuminen Loop Seal APROS-simulaatioissa. Espoo: VTT Technical Research Centre of Finland.

Hänninen, M. 2008. The one-dimensional separate two-phase flow model of Apros. Espoo: VTT. ISBN 978-951-38-7224-3 (nid.).

Hänninen, M. & Ylijoki, J. 2005. THE CONSTITUTIVE EQUATIONS OF THE APROS SIX-EQUATION MODEL.

Hänninen, M. & Ahtinen, E. 2009. Simulation of non-condensable gas flow in two-fluid model of APROS – Description of the model, validation and application. Annals of Nuclear Energy, 10, Vol. 36, No. 10, pp. 1588-1596. ISSN 0306-4549. doi: DOI: 10.1016/j.anucene.2009.07.018.

Hölzer, B. 1977. Specification of OECD standard problem No. 6, GRS-Garching, Battelle-Frankfurt.

Ishii, M. & Hibiki, T. 2006 . Thermo-Fluid Dynamics of Two-Phase Flow. Springer US.

Kolev, N.I. 2007. Multiphase Flow Dynamics 2: Thermal and Mechanical Interactions. Vol. 3rd Edition. Berlin, Heidelberg: Springer-Verlag. ISBN 9783540698357.

Kymäläinen, O. 1992. The assesment of RELAP5/MOD2 Against IVO Loop Seal Tests. Imatran Voima Oy, Finland. NUREG/IA-0082.

Lee, N., Bajorek, S.M., Meyer, P.E., Schwartz, W.R. & Tauche, W.D. 1983. Phenomenological uncertainty during loop seal steam venting in a small break cold leg LOCA of a PWR. ASME paper 83-WT-104, .

Lee, N. 1987. Discussions on loop seal behavior during cold leg small break LOCAs of a PWR. Nuclear Engineering and Design, 2/1, Vol. 99, pp. 453-458. ISSN 0029-5493. doi: DOI: 10.1016/0029-5493(87)90141-5.

Liebert, J. 1998. UPTF experiment: Flow phenomena during full-scale loop seal clearing of a PWR. Nuclear Engineering and Design, Vol. 179, No. 1, pp. 51-64. ISSN 00295493.

Lockhart, R.W. & Martinelli, R.C. 1949. Proposed Correlation of Data for Isothermal Two-phase, Two-component Flow in Pipes. Chemical Engineering Progress, Vol. 45, pp. 39-48.

Mishima, K. & Ishii, M. 1980. Theoretical Prediction of Onset of Horizontal Slug Flow Journal of Fluids Engineering, Vol. 102, No. 4, pp. 441-445. doi: 10.1115/1.3240720.

Ohvo, J. 1998. Ydinvoimalaitosten ensiöpiirin vesilukkojen käyttäytymisen tutkiminen.

Siikonen, T. & Kantee, H. 1983. Mixture level simulation using RELAP5/MOD1. First Proceedings of Nuclear Thermal Hydraulics 1983 Winter Meeting. American Nuclear Society. Pp. 281.

Taitel, Y. & Dukler, A.E. 1976. A model for predicting flow regime transitions in horizontal and near horizontal gas-liquid flow. AICHE Journal, Vol. 22, No. 1, pp. 47-55. ISSN 1547-5905. doi: 10.1002/aic.690220105.

Tuomisto, H. 1988. Two-phase flow in a full-scale loop seal facility. Nuclear Engineering and Design, Vol. 107, No. 3, pp. 295-305. ISSN 00295493.

Wallis, B. 1968. Phenomena of liquid transfer in two-phase dispersed annular flow. International Journal of Heat and Mass Transfer, Vol. 11, No. 4, pp. 783-785. ISSN 0017-9310.

Wallis, G. 1969. One-dimensional two-phase flow. New York: McGraw-Hill. ISBN 0-07-067942-8.

Wallis, G.B. & Dodson, J.E. 1973. The onset of slugging in horizontal stratified air-water flow. International Journal of Multiphase Flow, 10/10, Vol. 1, No. 1, pp. 173-193. ISSN 0301-9322. doi: DOI: 10.1016/0301-9322(73)90010-4.

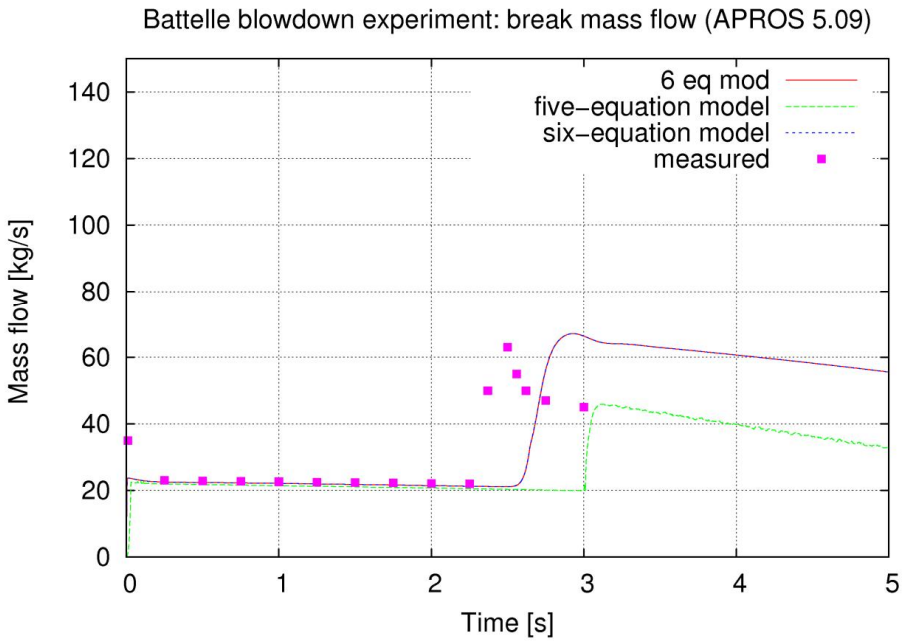
Battelle blowdown experiment: break mass flow (APROS 5.09)
6 eq mod
five−equation model
six−equation model
measured
Mass flow [kg/s]
Time [s]
0
20
40
60
80
100
120
140
0
1
2
3
4
5

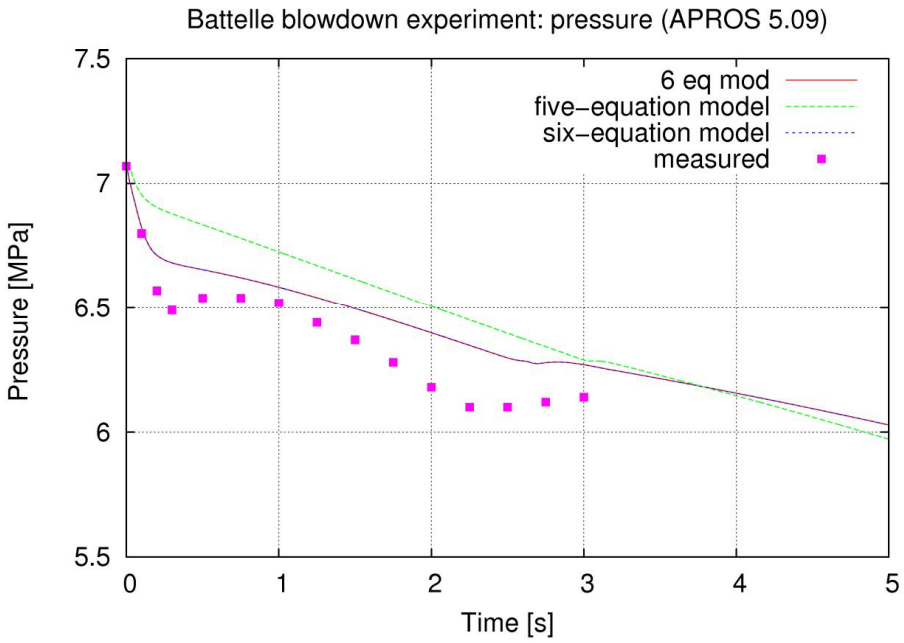
Battelle blowdown experiment: pressure (APROS 5.09)
6 eq mod
five−equation model
six−equation model
measured
Pressure [MPa]
Time [s]
5.5
6
6.5
7
7.5
0
1
2
3
4
5

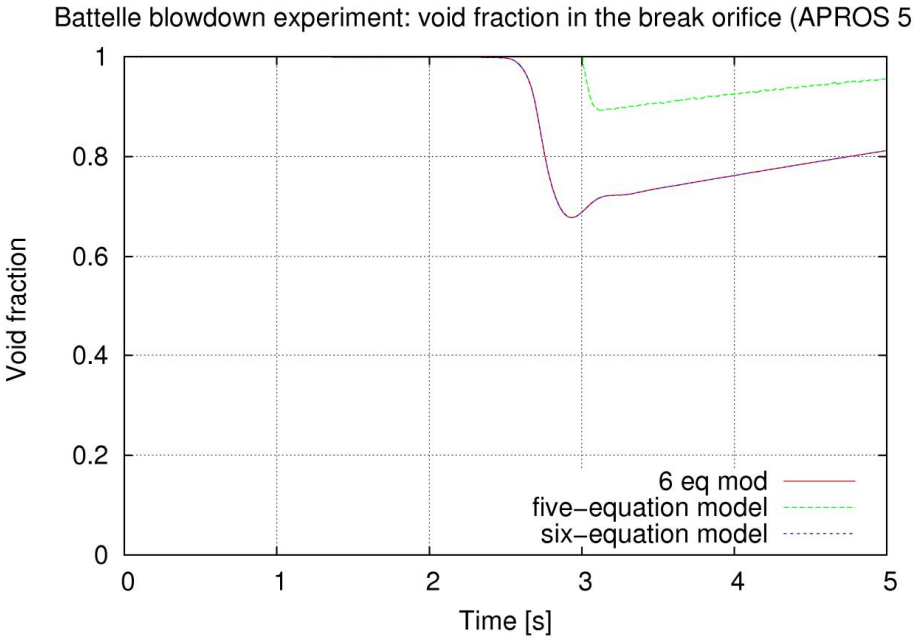
Battelle blowdown experiment: void fraction in the break orifice (APROS 5.09)
Void fraction
Time [s]
6 eq mod
five−equation model
six−equation model
0
0.2
0.4
0.6
0.8
1
0
1
2
3
4
5

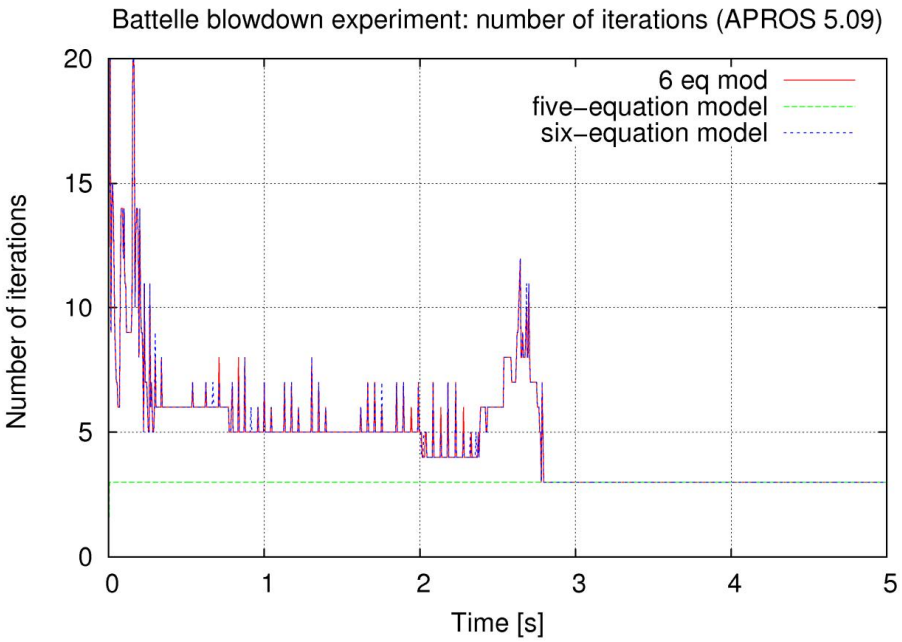
Battelle blowdown experiment: number of iterations (APROS 5.09)
Number of iterations
Time [s]
6 eq mod
five−equation model
six−equation model
0
5
10
15
20
0
1
2
3
4
5

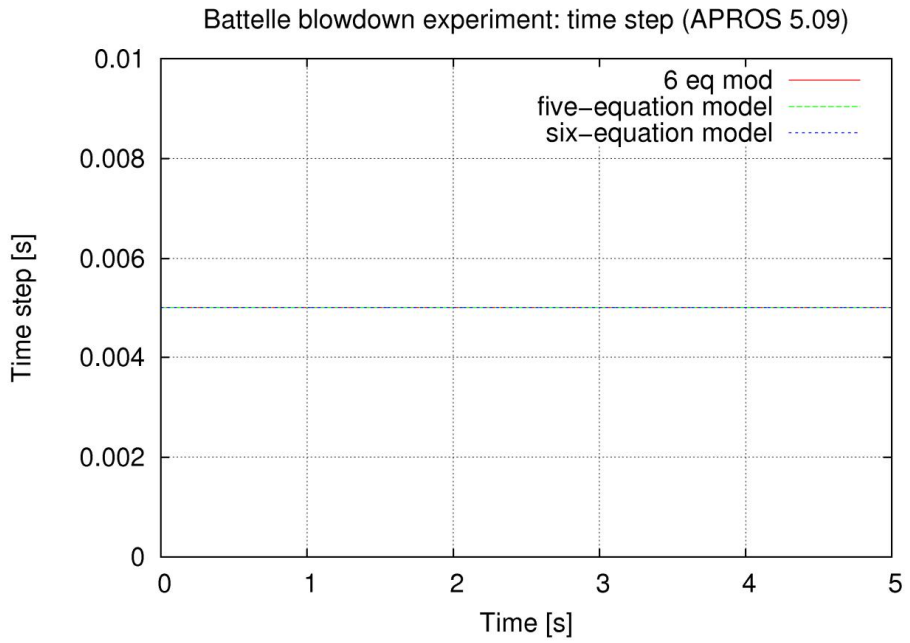
Battelle blowdown experiment: time step (APROS 5.09)
Time step [s]
Time [s]
6 eq mod
five−equation model
six−equation model
0.01
0.008
0.006
0.004
0.002
0
0
1
2
3
4
5

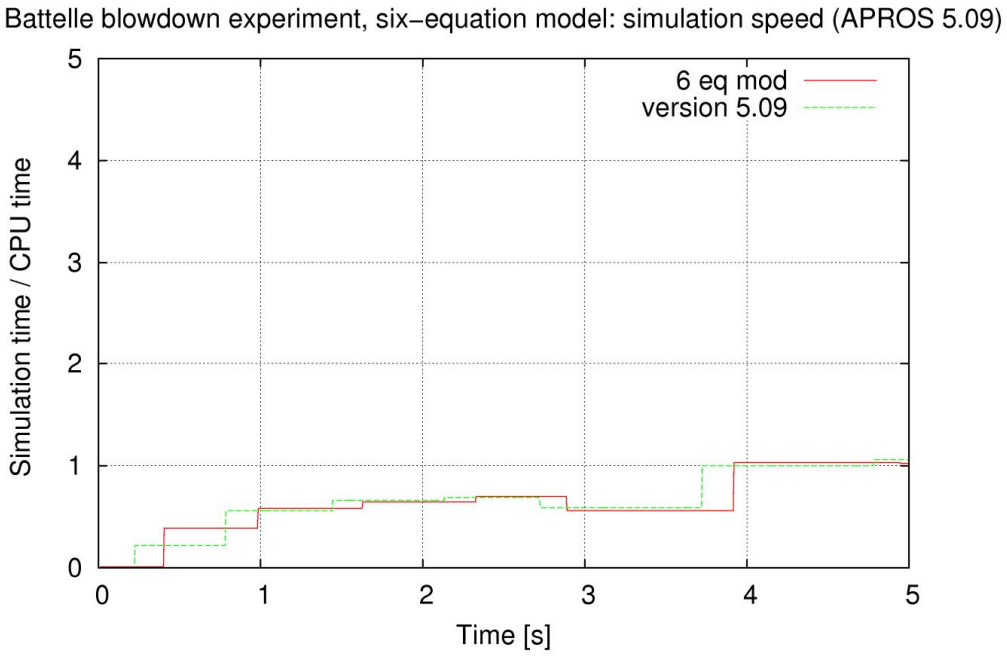
Battelle blowdown experiment, six−equation model: simulation speed (APROS 5.09)
Simulation time / CPU time
Time [s]
6 eq mod
version 5.09
5
4
3
2
1
0
0
1
2
3
4
5

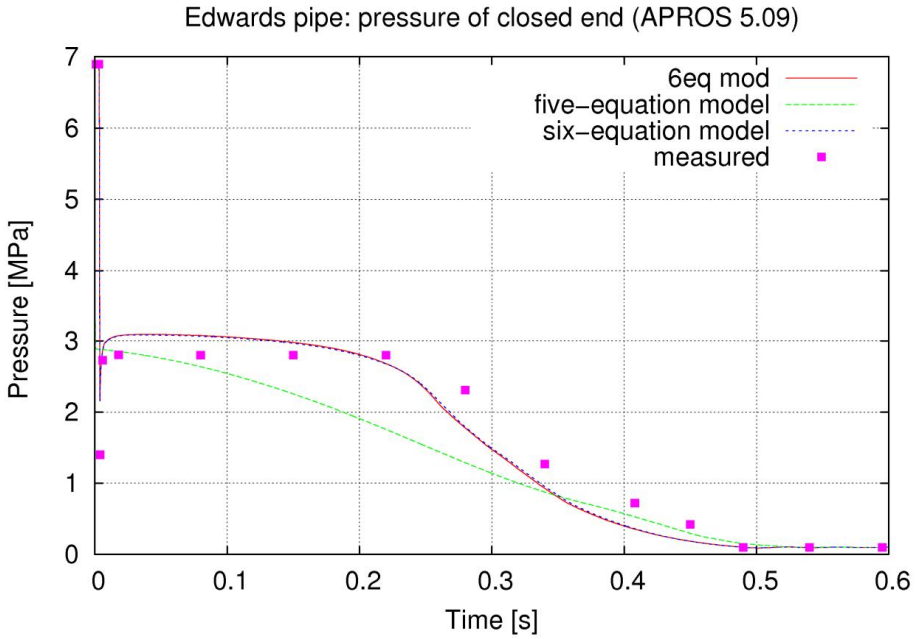
Edwards pipe: pressure of closed end (APROS 5.09)
6eq mod
five−equation model
six−equation model
measured
Pressure [MPa]
Time [s]
0
1
2
3
4
5
6
7
0
0.1
0.2
0.3
0.4
0.5
0.6

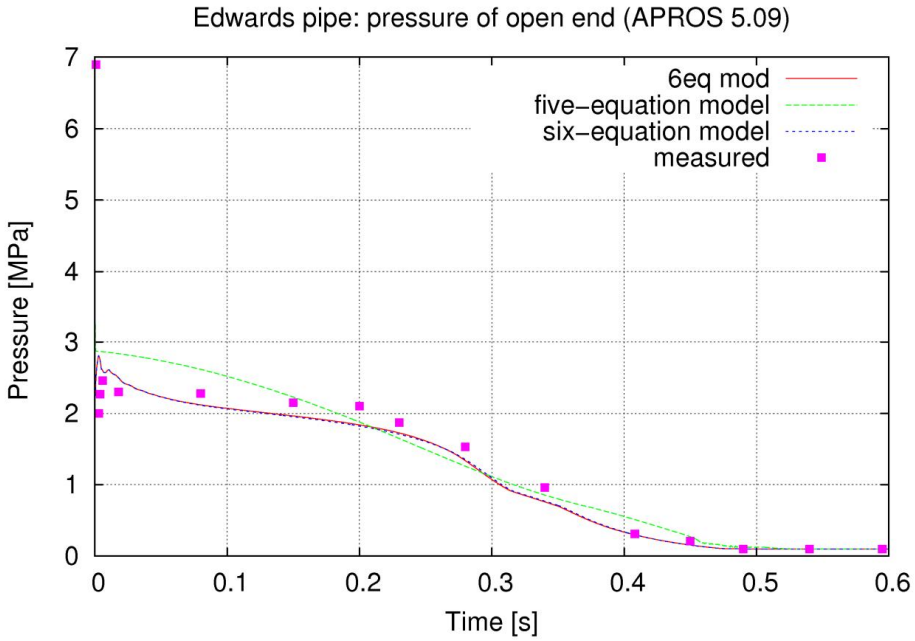
Edwards pipe: pressure of open end (APROS 5.09)
6eq mod
five−equation model
six−equation model
measured
Pressure [MPa]
Time [s]
0
1
2
3
4
5
6
7
0
0.1
0.2
0.3
0.4
0.5
0.6

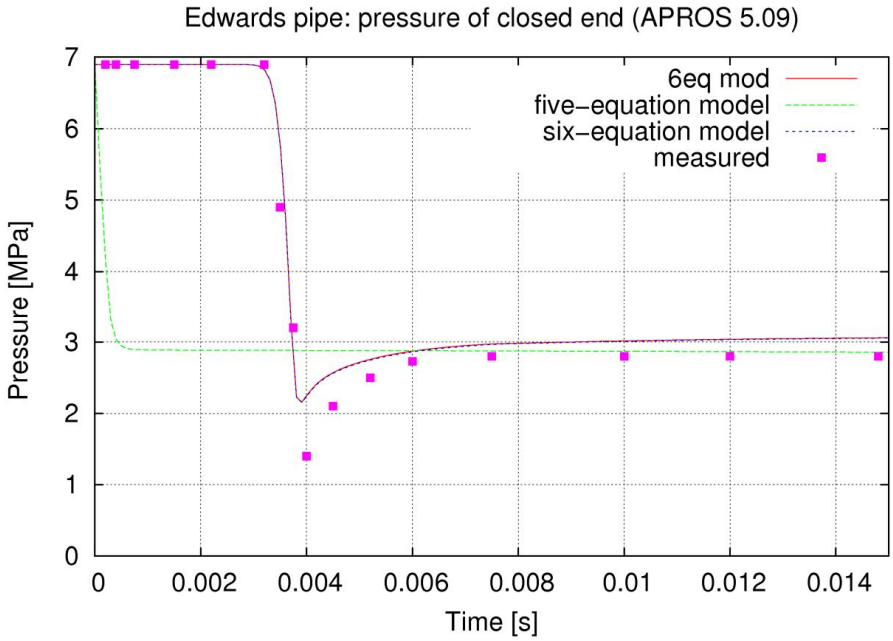
Edwards pipe: pressure of closed end (APROS 5.09)
6eq mod
five−equation model
six−equation model
measured
Pressure [MPa]
Time [s]
0
1
2
3
4
5
6
7
0
0.002
0.004
0.006
0.008
0.01
0.012
0.014

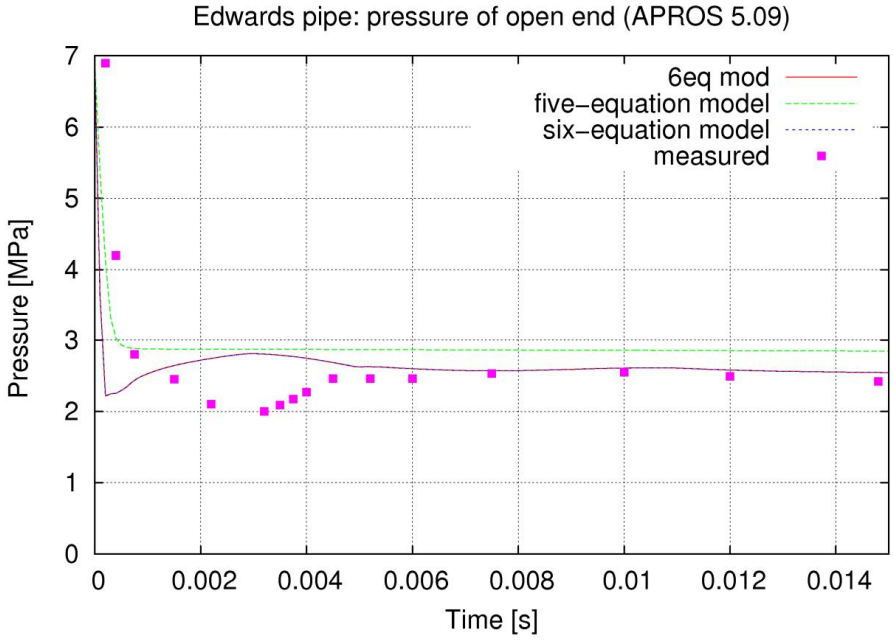
Edwards pipe: pressure of open end (APROS 5.09)
6eq mod
five−equation model
six−equation model
measured
Pressure [MPa]
Time [s]
0
1
2
3
4
5
6
7
0
0.002
0.004
0.006
0.008
0.01
0.012
0.014

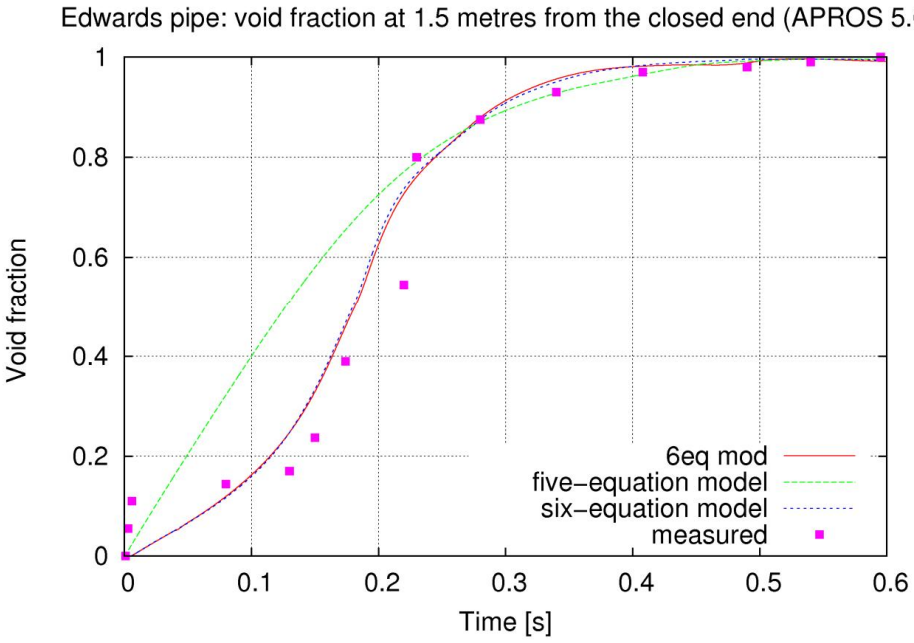
Edwards pipe: void fraction at 1.5 metres from the closed end (APROS 5.09)
Void fraction
Time [s]
6eq mod
five−equation model
six−equation model
measured
0
0.2
0.4
0.6
0.8
1
0.1
0.3
0.5

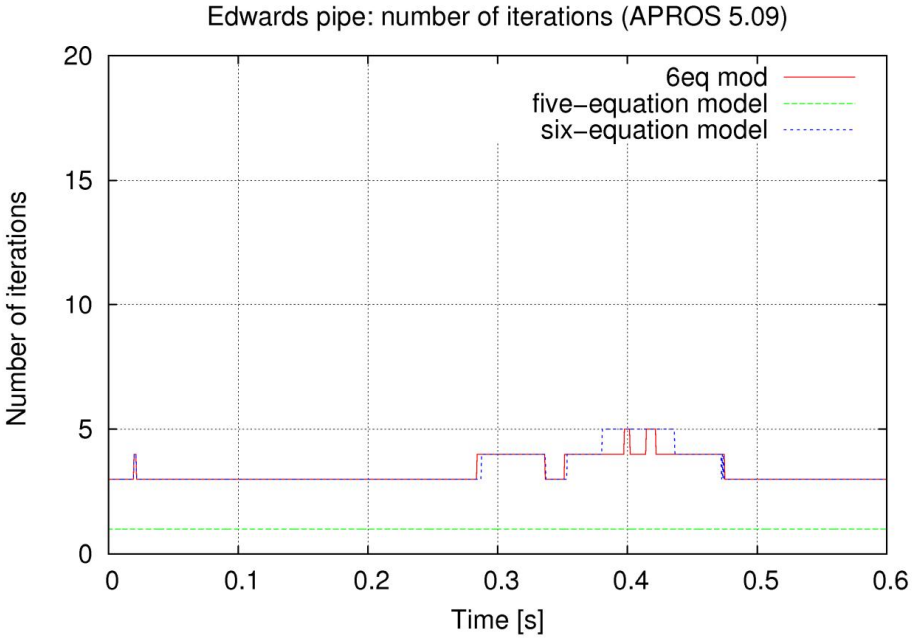
Edwards pipe: number of iterations (APROS 5.09)
Number of iterations
Time [s]
6eq mod
five−equation model
six−equation model
0
5
10
15
20
0.1
0.2
0.3
0.4
0.5
0.6

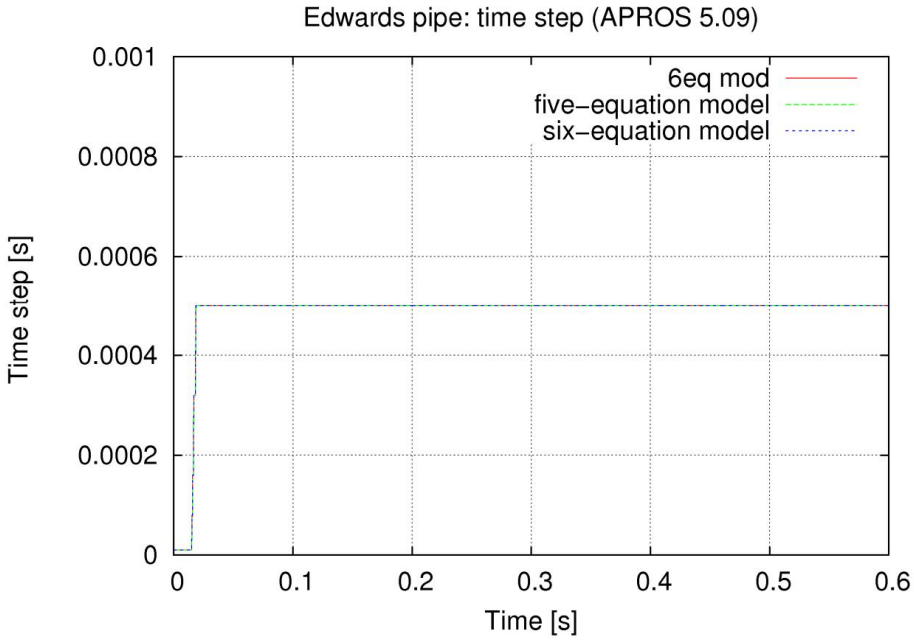
Edwards pipe: time step (APROS 5.09)
Time step [s]
Time [s]
0.001
0.0008
0.0006
0.0004
0.0002
0
0
0.1
0.2
0.3
0.4
0.5
0.6
6eq mod
five−equation model
six−equation model